2016

Novel Small Airway Model Using Electrospun Decellularized Lung Extracellular Matrix

Bethany M. Young
VCU

Virginia Commonwealth University

This is to certify that the thesis prepared by Bethany Young entitled "Novel Small Airway Model Using Electrospun Decellularized Lung Extracellular Matrix" has been approved by her committee as satisfactory completion of the thesis requirement for the degree of Master of Science in Biomedical Engineering.

Dr. Rebecca L. Heise, Assistant Professor

Dr. David Simpson, Associate Professor

Dr. Hu Yang, Associate Professor

Dr. Ning Zhang, Associate Professor

Dr. Henry J. Donahue, Chair of Biomedical Engineering

Dr. Barbara Boyan, Dean of the School of Engineering

Dr. F. Douglas Boudinot, Dean of the School of Graduate Studies

NOVEL SMALL AIRWAY MODEL USING ELECTROSPUN DECELLULARIZED LUNG EXTRACELLULAR MATRIX

A Thesis submitted in partial fulfillment of the requirements for the degree of Master of Science in Biomedical Engineering at Virginia Commonwealth University

by

BETHANY MARIE YOUNG
Bachelors of Science, University of Richmond, 2014

Director: REBBECCA L. HEISE, PH. D.
Assistant Professor, Biomedical Engineering

Virginia Commonwealth University
Richmond, Virginia
May, 2016

Acknowledgement

I would first like to thank Dr. Rebecca Heise for all of your guidance and encouragement. I have learned so much through this experience with you as a mentor. Thank you very much for allowing me to come into this lab as an undergraduate and being supportive throughout the past 2 years.

I would also like to extend my appreciation to Dr. Hu Yang, Dr. Ning Zhang, and Dr. David Simpson for being a part of my committee. As well as all of the other members of the Heise Lab, Brittany Allen, Robert Pouliot, Joe Herbert, Mike Valentine, Patrick Link, Adam Blakeney, Monika Radhika, Matt Schneck, Nabil Mikhaiel, Franck Kamaga Gninzeko, and Alex Ratti for all of your help and support.

Several facilities helped me greatly with guidance and equipment, including VCU Department of Anatomy and Neurobiology Microscopy Facility, VCU Nanomaterials Core Characterization Facility, Dr.Yang's Lab for help with electrospinning and mechanical testing, and Dr. Zhao's lab for help with contact angle measurement.

Lastly, I would like to thank my family for their endless generosity and love through all of my education. You guys made it possible for me to be here and I appreciate everything you've done. A special shout out to my boyfriend, Ben Fowler, for being so understanding throughout this experience, supporting me emotionally and financially, and overall just being the best boyfriend. Thank you and I love you all!

Table of Contents

List of Tables

Page

List of Figures

Page

Abstract

NOVEL SMALL AIRWAY MODEL USING ELECTROSPUN DECELLULARIZED LUNG EXTRACELLULAR MATRIX

By Bethany Marie Young B.S.

A Thesis submitted in partial fulfillment of the requirements for the degree of Master of Science at Virginia Commonwealth University.

Virginia Commonwealth University, 2016

Major Director: Rebecca L. Heise Ph. D.

Assistant Professor, Biomedical Engineering

Chronic respiratory diseases affects many people worldwide with little known about the mechanisms diving the pathology, making it difficult to find a cure. Improving the understanding of smooth muscle and extracellular matrix (ECM) interaction is key to developing a remedy to this leading cause of death. With currently no relevant or controllable *in vivo* or *in vitro* model to investigate diseased and normal interactions of small airway components, the development of a physiologically relevant *in vitro* model with comparable cell attachment, signaling, and organization is necessary to develop new treatments for airway disease. The goal of this study is to create a mechanically, biologically and structurally relevant *in vitro* model of small airway smooth muscle tissue. Synthetic Poly-L-Lactic Acid (PLLA) and decellularized pig lung ECM (DPLECM) were electrospun to form nanofibrous mats that can closely mimic natural bronchial tissue. The addition of DPLECM significantly changed the PLLA scaffold mechanically, biologically, and physically to bring it closer to the characteristics of the human lung. DPLECM scaffolds exhibited a significant decrease in the elastic modulus compared with PLLA alone. Histological staining and SDS-PAGE showed that after scaffold fabrication, essential proteins or protein fragments in natural ECM are still present after processing. Human bronchial smooth muscle cells (HBSMCs) seeded onto PLECM scaffolds formed multiple layers of cells compared to scaffolds composed solely of PLLA. Phenotype of smooth muscle is better maintained when DPLECM is incorporated into the scaffold shown by enhanced contractile protein expression and increased collagen production for normal smooth muscle remodeling of the scaffold. In summary, this research demonstrates

that a PLLA/DPLECM composite electrospun mat is a promising tool to produce an *in vitro* model with the potential to uncover unknown characteristics of bronchiole smooth muscle behavior in diseased or normal states.

CHAPTER 1: INTRODUCTION

Airway Anatomy and ECM

The structure of the lungs consists of many branched airways that allow for air to travel to the alveoli for gas exchange while being heated and conditioned. The first region of branching is considered the conducting zone and consists of the trachea, bronchi, and the bronchioles. The final zone is responsible for gas exchange and is therefore called the respiratory zone comprised of respiratory bronchioles, alveolar ducts and alveoli [1].

The natural cellular population within the respiratory tract is lined with ciliated cells which are pseudostratified columnar in the upper airways and cuboidal closer to the terminal bronchioles. Ciliated cells function as a defense system, moving debris and mucus from the airways by pulsatile beating. Interspersed with the ciliated cells in the larger airways, there are goblet cells that are responsible for mucus secretion. Moving to the smaller airways, these cells are replaced by Clara cells that secrete other proteins such as surfactant and inflammatory molecules [2]. Another type of cell found in the airways are mast cells that are involved in the secretion of many inflammatory mediators to cause bronchoconstriction, mucus secretion, and modifying the permeability of the surrounding blood vessels [2]. In the alveoli, the epithelial layer is composed of squamous type I alveolar cells with fewer cuboidal type II alveolar cells [2]. Type II alveolar cells are progenitor cells for alveolar type I epithelium [1] and also produce surfactant to reduce surface tension within the alveoli.

Airway structure closely resembles the cardiovascular system in that they are designed to withstand shear forces created by air instead of blood and with smooth muscle contraction to control the movement and pressure [3]. ECM components and their placement around the airways are important to keep a constant airway compliance for natural airway physiology. The airway walls are divided into layers. The first layer is the mucosa that surrounds the lumen of the airway. It is comprised of epithelium, basement membrane, and subepithelial collagen [4]. The basement membrane lies directly underneath a layer of epithelial cells and is composed of collagen type-IV, laminin, entactin/nidogen, and heparin sulfate [3]. Beyond the basement membrane, there is a section in the mucosa composed of collagen type III and V and laminin that is considered the subepithelial collagen. This section functions to give structural support to the airways [3]. Beyond the mucosa layer there is the submucosa layer that is comprised of mostly collagen, elastin, and proteoglycans and is the region where most fibroblasts and smooth muscle cells are found [3]. The overall organization of the cells and structural proteins as it progresses down the airways to the alveoli can be seen in Figure 4.

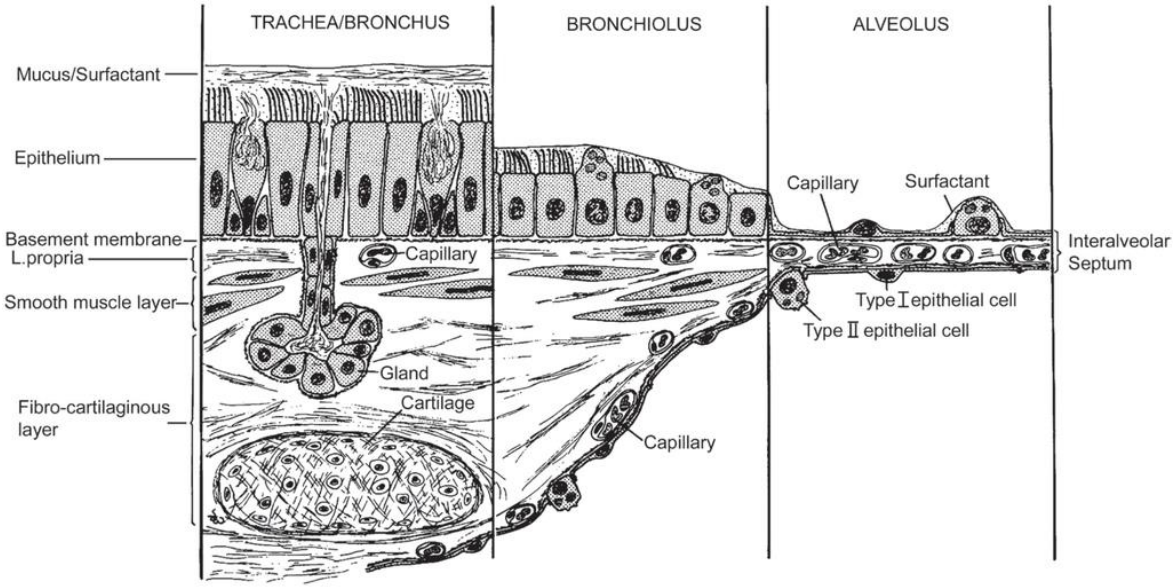

Figure 1: Airway wall organization. Airway wall cross-section showing organization of cells and connective tissue from the trachea to the alveoli. Produced with permission from [4].

Asthma and COPD

Two major debilitating obstructive airway diseases are bronchial asthma and chronic obstructive pulmonary disease (COPD). Asthma currently effects 300 million people worldwide with expectations for it to effect 400 million people by 2025 [5]. COPD, similarly, is expected to become the third leading cause of death by 2020 [6]. Both of these diseases are characterized by a severe inflammatory response to allergens and structural remodeling of the airway wall leading to chronic symptoms [6], [7].

A factor distinguishing asthma from other airway diseases is the reversibility of the airway narrowing with removal of activity and allergens or medications [8]. Asthma affects all conducting airways of the lungs with over stimulation of the airway smooth muscle (ASM), severe inflammation, and mucus secretion causing constriction of airflow

and difficulty breathing [9]. These pathologies are in response to various internal and external stimuli including airborne allergens, infection, exercise, cold air, smoke, beta blockers, and stress [9], [10]. If left untreated, asthma can cause many more irreversible changes in lung tissue. Edema is a key component of prolonged asthma, it is initiated when long term inflammation dilates blood vessels causing fluid and protein leaking into the surrounding tissue [11]. If edema and inflammation persists, fibrosis may develop with even more weakening symptoms. Smooth muscle modulation is another key prolonged effect of asthma. Inflammatory cells release signaling molecules that can stimulate smooth muscle growth, hyperactivity [11], and remodeling of the structural elements of the lung [9]. Asthma can be difficult to treat and study because of the variation between patients. Since there are many different causes and responses to therapy, there is a large impact of genes on the asthmatic response [9].

COPD, in comparison, is a term that encompasses emphysema, chronic bronchitis and some bronchiectasis, but mostly describes irreversible airway limitation caused by abnormal inflammatory response to environmental factors or genetic signaling [12], [13]. Differing from asthma, COPD occurs almost exclusively in the smaller airways, making it less accessible for biopsies [13]. Most symptoms that contribute to the inflammatory response include structural changes of small airway ways such as epithelial metaplasia, increased ASM mass, goblet cell increase, and submucosal gland hypertrophy and secretion [13]. In comparison to asthma, COPD is much less understood from the perspective of the molecular mechanisms that drive the pathology. Diagnosis of COPD from asthma is usually distinguished by lung functional testing or if patient has exposure to

environments with toxins known to cause COPD [6]. Lung testing is done to examine the ratio of forced expiratory volume in one second (FEV_1) to forced vital capacity (FVC) [6]. In this ratio, there is a significantly decreased FEV_1 [13] causing the patient to exert more force to inflate the lungs. Individuals can also be diagnosed based on the risk factors caused by prolonged inhalation of noxious gases, smoking, or toxic gasses or pollution [6].

Although there are many overlapping symptoms between the two diseases there are many differences still undiscovered. The major difference between the two diseases is seen in the inflammatory response, airway hyperresponsiveness [6], [14] and cellular recruiting. Summary of similarities and differences between COPD and asthma, in airway remodeling, symptoms, and inflammatory response are seen in Figure 2. One of the largest gaps in information in both diseases is the inflammatory characteristics that differ between the two [15]. The differences in inflammatory response are easily seen by the recruitment of different inflammatory cells and mediators to the airways at different times. Asthma has an increased number of activated CD4+ T-lymphocytes, eosinophils, and mast cells while in COPD there is an increased number of CD8+ T-lymphocytes, macrophages and neutrophils [15], [16]. Although these differences are prevalent, there is much more to be discovered about the cellular and molecular mechanisms driving asthma and even more to be understood about COPD [15], [17]. By unveiling the mechanisms behind these diseases, opportunities will arise for pharmacological solutions. Asthma's symptoms are typically managed with corticosteroid therapy, but there is no specific treatment for COPD and therefore is treated as a less responsive form of asthma [15]. To increase the knowledge

and therefore cures for these diseases, a more feasible option to study diseased and natural states in these regions needs to become available.

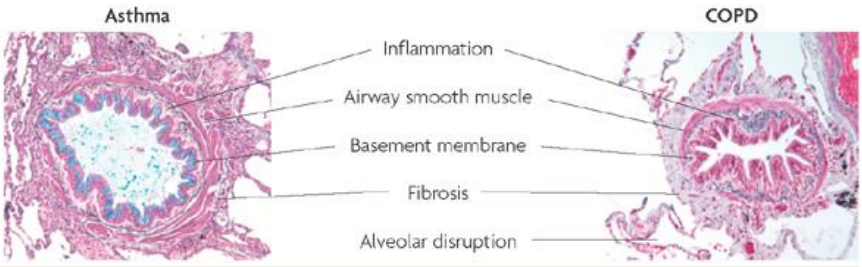

Inflammation	+++	+++
Airway smooth muscle	+++	+
Basement membrane	++	–
Fibrosis	+ (subepithelial)	+++ (peribronchiolar)
Alveolar disruption	–	+++
Airway vessels	++	No change
Mast cells	++ (and activated)	Normal
Dendritic cells	++	ND
Eosinophils	++	Normal
Neutrophils	Normal	++
Lymphocytes	T_H2 type	T_H1 and T_C1 type
Epithelium	Often shed	Pseudostratified
Goblet cells	++	++

Nature Reviews | Immunology

Figure 2. Similarities and differences between COPD and Asthma with respect to inflammatory response, airway wall changes, and symptoms. Reproduced with permission from [16].

Airway Smooth Muscle Background

Airway smooth muscle (ASM) plays a key role in lung homeostasis and disease pathologies. It is found from the trachea to the terminal bronchioles and is responsible for bronchomotor tone [17]. From a physiological prospective, there is no imperative purpose for airway smooth muscle dilation, the only function of ASM seems to be an undesirable

pathological drawback [18]. Change in structure and arrangement from the upper airways to lower airways is seen in various ways. In the upper airways, ASM is found attached to the cartilage in the posterior region while in the lower airways it is seen in a helix-antihelix arrangement around the bronchi [17]. There has also been research to show that there is a difference in the distribution of B-adrenergic receptor expression in the two regions [17], possibly giving foresight into why asthma occurs in all regions of the lung but COPD mostly only occurs in the lower airways. The complexity and specialization of ASM in various regions, lead us to believe there is a purpose for its contraction that has not yet been discovered and it differs from region to region.

The basic mechanisms of ASM contractility include the well-known actin myosin crossbridge cycling present in all muscle types but there is also a more complex interaction of the actin filaments with extracellular proteins. Actin filaments indirectly bind to membrane adhesion plaques through molecular complexes, such as alph-actinin, talin and filamin. It is those molecular complexes that bind to adhesion plaques, which then bind to integrin proteins of the ECM in the configuration seen in Figure 3, to transmit external forces inside of the ASM cells [19].

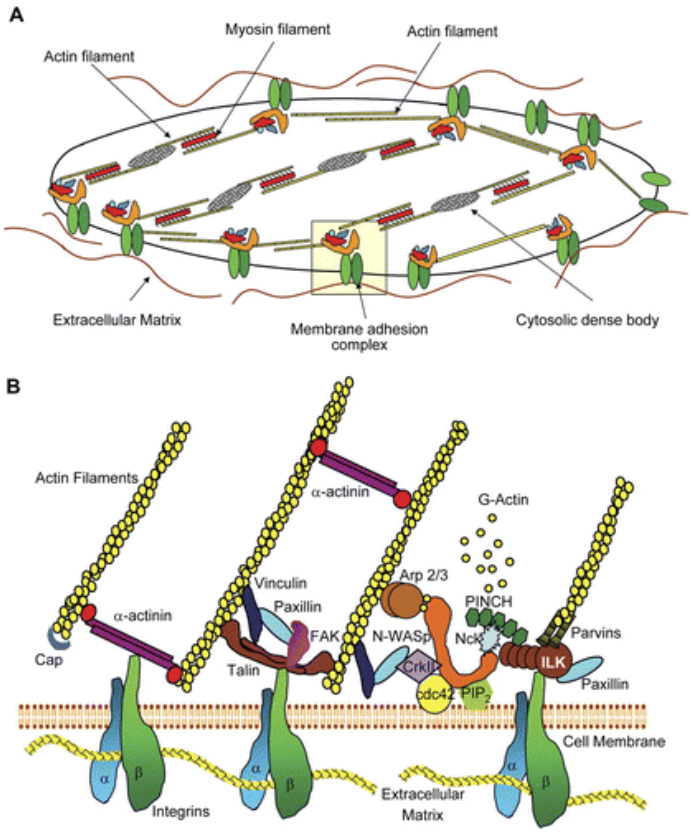

Figure 3. Airway smooth muscle cytoskeletal protein arrangement and attachment to ECM molecules. A) Arrangement of Actin and myosin within the cell and overview of actin attachment to membrane adhesion complexes and ECM. B) Detailed binding of Actin filaments indirectly to adhesion complexes and ECM proteins through various molecules. Reproduced with permission from [19].

ASM can create metalloproteinases to destroy old matrix and then lay down various ECM proteins. The ratio and abundance of ECM proteins can differ in ratio and abundance based on the inflammatory and mechanical signals it is receiving from the environment [17]. If signals for disease have been transcribed in the ASM cells during a diseased state, it can encourage ASM growth as well as ECM production with qualities

different from normal airway ECM. Cellular differentiation is specifically modulated by ECM through variations in mechanical forces transduced by adhesions sites [17].

Major phenotypic changes can be seen in ASM during diseased states based on surrounding environment including the contractile protein expression such as alpha-actin, myosin heavy chain, and calponin [20], [21]. A more undifferentiated mesenchymal phenotype is seen from ASM exposed to unusual structural properties or signaling profile such as those seen in COPD and Asthma [17], [20]. Research has shown that ECM components such as laminin and collagen type IV can prolong the contractile phenotype of ASM cultured *in vitro*, as well as keep normal proliferation levels as compared to cells seeded without vital ECM components [20], [21].

Overall it is understood that ASM is drastically influenced by mechanical forces, ECM signaling, and inflammatory signaling. Any modulation to these factors can influence the expression of phenotypic markers, leading to airway disease such as asthma or COPD. There has been evidence that ASM undergoes modulation in diseases such as asthma and COPD [17]. Many factors affect the narrowing of the airways involved in asthma but there have been shown to be abnormalities in airway smooth muscle structure and function and increased smooth muscle mass causing smooth muscle hyperresponsiveness [8]. Because of ASMs influence on the homeostasis of airway tissue, fully understanding the modulating factors may create more opportunities for therapy.

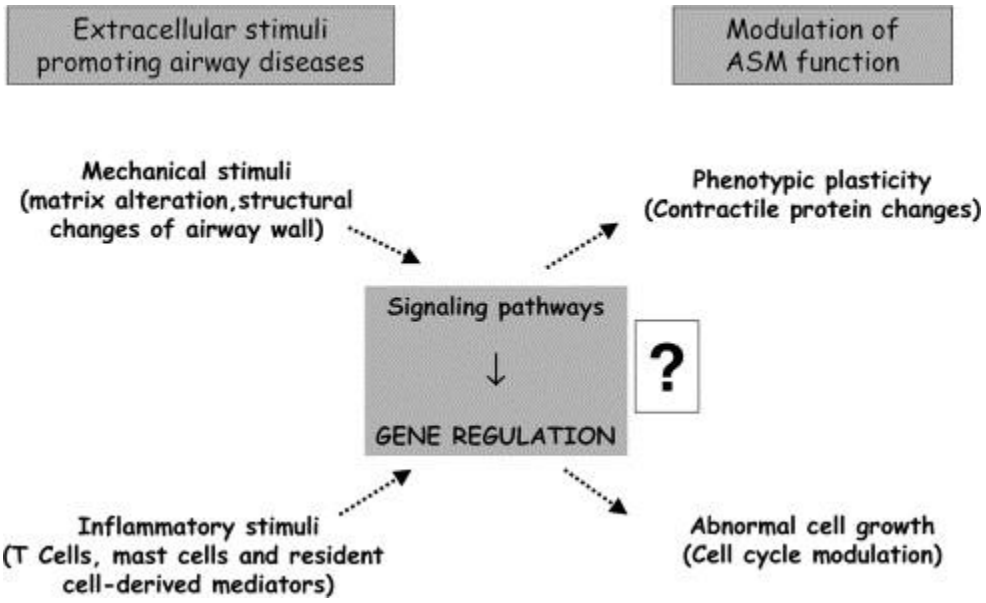

Figure 4: Overview of ASM phenotypic modulation through abnormal environmental stimulation during diseased states, highlighting the region of therapeutic intervention from signaling pathways to gene regulation. Reproduced with permission from [17].

Current Strategies for Airway Modeling

Current studies associated with COPD and asthma lack a good animal model affecting the possible level of understanding of the cellular and molecular mechanisms driving ASM hyper-reactivity. Data we have today focuses on research with whole airways or investigations of isolated monolayered ASM cells. There are downfalls of both approaches including the lack of biological insight with whole airway sample and the deficiency of structural and environmental ques in a single cell investigation. Platforms for lung tissue modeling presently lack several key physiological characteristics existing in the natural lung. These are commonly studied on two dimensional tissue culture plastic or other two dimensional rigid surfaces lacking the proper environment of natural tissue.

Creating a reliable and accurate in vitro model of the small airways has rarely been done and will offer a controllable and highly observable platform for studying intracellular pathways in normal tissue remodeling and diseased states. Another benefit of completing this goal is to decrease the reliance on animal models for cost and moral purposes. This method enables the use of human cells in vitro, which have proven more accurate than the use of mice or other animals with physiological and anatomical differences [17].

A useful strategy when modeling a cellular environment is to closely mimic the surrounding ECM. One effective way to imitate the structure of ECM is through electrospinning. Electrospinning is a highly controllable and versatile technique using high electric potentials to develop nano or mico sized fibers that mimic natural fibers throughout the human body [22]. More specifically, the polymer solution is forced out of the needle tip by an electrical charge differential until a Taylor cone is formed and creates a stream of fluid directed towards the grounded target as seen in Figure 5. This technique creates fibers ranging from a few nanometers to micrometers, which resembles the range of fiber diameter has to natural ECM protein diameter and arrangement [23]. This fiber distribution makes it an attractive process for tissue engineering. There are many variations that can be added to the electrospinning process to tailor it for different applications. Changes in characteristics such as fiber size, alignment, mechanical properties or porosity [24] can be changed by varying parameters of the electrospinning set up. To create a nanofibrous scaffold with random alignment the set up shown in Figure 5 is used. When layered randomly into a three dimensional mat, the resulting scaffold has a highly porous

architecture allowing nutrient movement, cell infiltration, and a multiaxial mechanical strength.

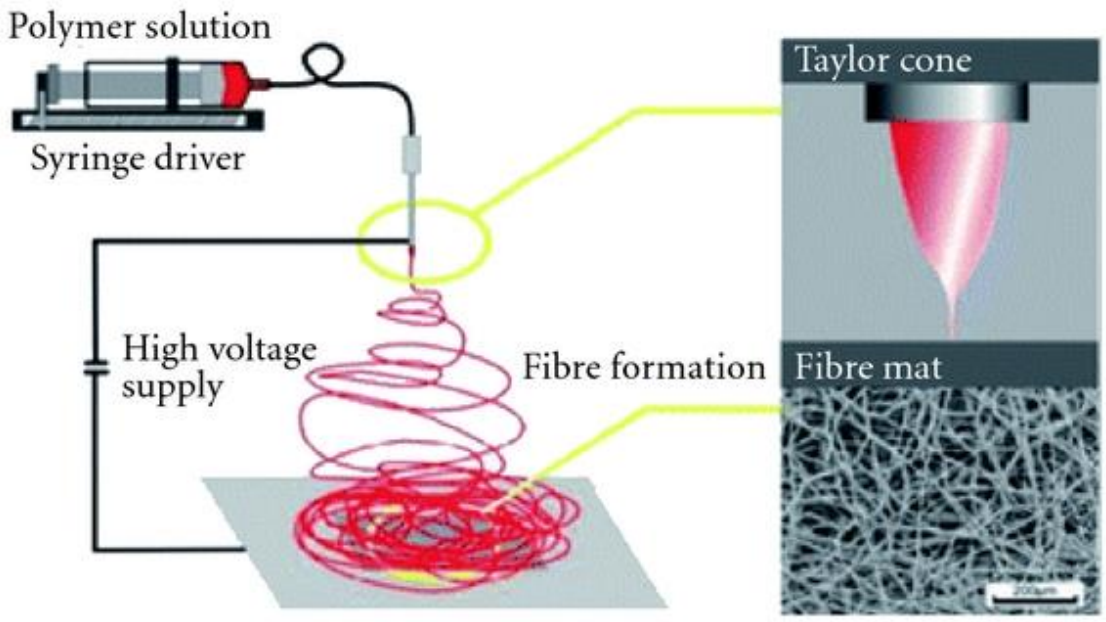

Figure 5: Conventional electrospinning set up. Plastic syringe containing polymer and volatile solvent solution that is to a voltage supply, to create a Taylor cone and jet of polymer to deposit onto a grounded metal mandrel. A randomized fibrous mat is created as seen by SEM. Reproduced with permission from [25].

Variations to the basic electrospinning process allows for the application of this process to a broad range of uses. For example, the choice of material can change mechanical properties, bioactivity, and electrospinning parameters. When making a viable cellular model, the first goal is to create a biologically active material with strength similar to that of natural lung tissue. This can be done by combining a naturally derived substance

with a synthetic polymer. Incorporating natural ECM substances into scaffolds have the potential to promote constructive tissue remodeling after injury in many areas of tissue engineering including vascular [26], skeletal muscle [27], and central nervous systems[28]. These materials offer more similarities to lung tissue than exclusively synthetic scaffolds because of the cellular attachment and tissue-specific signaling that take place with natural extracellular matrix (ECM) proteins (i.e. collagen, elastin, fibronectin, and laminin). Research has been done incorporating collagen [29], [30], gelatin [31], fibrinogen [32], and many other combinations of natural proteins to increase biocompatibility. Cellular recognition of the native tissue ECM decreases inflammatory response to create the environment needed for constructive remodeling [33]. Specifically, the degradation products generated by the ECM proteins recruit cells and induce proliferation that encourages scaffold remodeling [34].

The cell-matrix interaction can also be optimized by tailoring the fiber size to mimic the environments surrounding specific cell types. For example, epithelial tissue prefers a dense, smaller fiber scaffold to resemble the basement membrane. In comparison, smooth muscle cells and fibroblasts prefer a larger fiber diameter with increased porosity [35]. There has been research creating models using this idea that different cells need different structural environments. In research that includes more than one cell type, variations in structural environments were achieved with biphasic scaffolds [35], [36].

It is also important to note that ECM is not uniform across all tissue in the body, and the dissimilarities determine cell behavior including the activation or deactivation of internal cell signaling [28]. Studies have shown that the origin of the natural ECM will

change MSC phenotype towards a lineage native to the original organ [37]. There is an ongoing feedback loop between the cells laying down ECM specific to cell phenotype and the ECM signaling the cells towards a specific tissue phenotype [27]. In this research we propose that for these reasons, decellularized porcine lung ECM would offer the appropriate signaling for proper phenotypic expression of lung cells [38]. To increase the mechanical strength that DPECM lacks, PLLA will be added to form a composite material to also offer, biocompatibility and workability.

Objectives:

The advantages of natural extracellular environment have been exploited in this study by incorporating decellularized ECM into electrospinning of an FDA approved, biodegradable [41] synthetic polymer. This offers customizable nanostructure, mechanical profile, and degradation properties with practical biological signaling optimized for an accurate human analog for smooth muscle function in the airways. This research aims to characterize the mechanical and microstructural properties of a naturally derived lung ECM and Poly-L_Lactic Acid (PLLA) electrospun nanofibrous fabric. The basic cell-scaffold interactions were examined with native lung cells to assure its future success. Confirming these properties could establish this material as a medium that stimulates lineage and tissue-specific interactions for airway cells. The goal of this study was to create a scaffold electrospun with PLLA and decellularized pig lung ECM (DPLECM) possessing increased biocompatibility compared to a PLLA scaffold.

Specific Objectives:

1. Fabricate PLECM/PLLA electrospun scaffold with randomized nanofibers.
2. Characterize properties of the scaffold.
    a. Assess fiber size through quantification of SEM images.
    b. Perform tensile testing on wet scaffolds with and without cells to compare to natural lung tissue.
    c. Asses hydrophobicity off electrospun scaffolds with PLECM to compare to PLLA only scaffolds
    d. Confirm the presence of ECM proteins or protein fragments after exposure to Hexafluoro-2-propanol (HFP) and electrospinning.
3. Assess biocompatibility by culturing primary cell lines
    a. Compare ASM cell attachment and morphology on scaffolds containing PLECM to pure PLLA scaffolds.
    b. Evaluate gene expression changes and morphology of ASM to confirm the maintenance of contractile phenotype in PLLA/PLECM model.

CHAPTER 2: Materials and Methods

2.1 Overview of Experimental Design.

Extracellular matrix (ECM) was extracted from porcine lungs, decellularized and pulverized through chemical and physical means to obtain an ECM powder. The ECM was then dissolved into hexafluoro-2-propanol (HFP) and Poly-L-lactic acid (PLLA) solutions at various concentrations and electrospun into a thin fibrous mat. Fibers and overall scaffold were characterized and evaluated for strength and biocompatibility with Human Bronchial Smooth Muscle Cells (HBSMCs). Optimum ECM/PLLA concentrations were previously found based on strength and ability to properly electrospin. All data is compared to a control of 100% PLLA nanofibers created under similar electrospinning parameters.

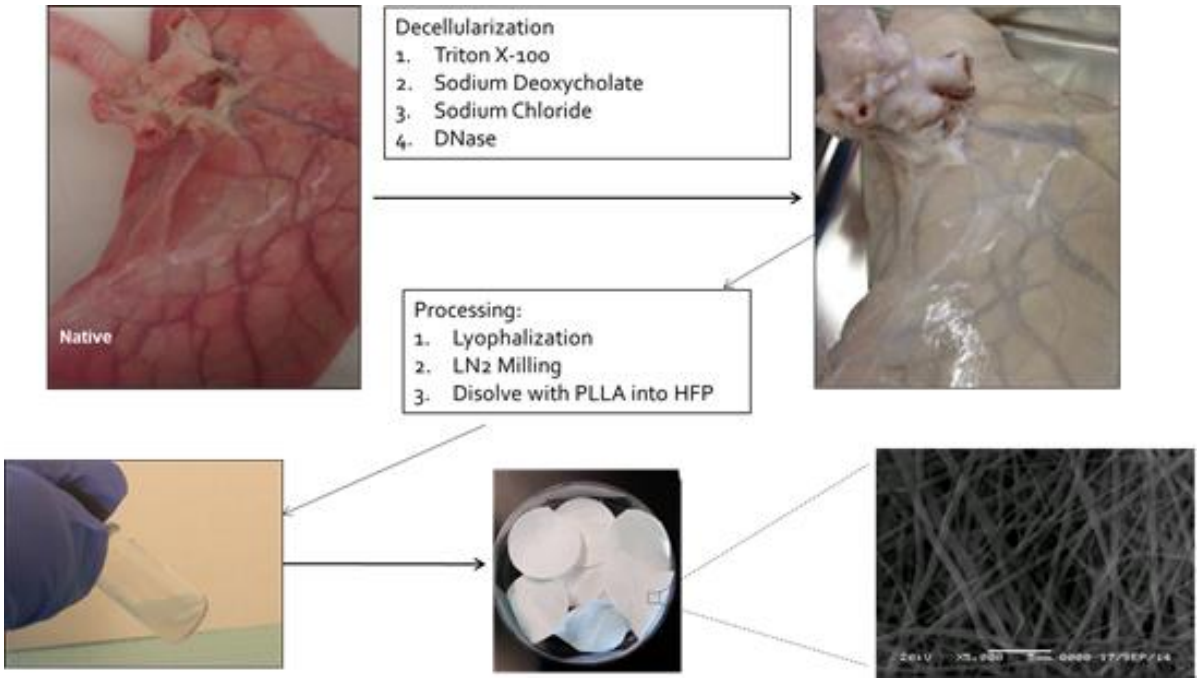

Figure 6: Processing steps of porcine lung tissue from cellular whole lung, depicted on the top left to a nanofibrous mat shown on the bottom right. The process starts with a chemical decellularization process to give a decellularized whole lung seen at the top left which is then physically milled to obtain a powder that is put into a PLLA/ECM/HFP solution seen at the bottom left. The solution is then electrospun into thin mats seen in the bottom center which are composed of nanofibers visible by SEM at the bottom right.

2.2 Porcine Lung Decellularization and Preparation

2.2.1 Tissue Decellularization.

Pig lungs (donated from Smithfield Hams) were decellularized by established protocol [39], [40]. The lung was perfused through the trachea and vasculature with sterile water containing penicillin/streptomycin (Life Technologies), before being drained passively. The lungs were then perfused with 0.1% Triton X-100 (Fisher Scientific) and submerged overnight before rinsing again with the water and penicillin/streptomycin solution. The lung was perfused with a 2% sodium deoxycholate (Sigma) solution for 24 hours, then directly filled with a DNase solution for one hour. The lung was rinsed before adding sodium chloride (Fisher Scientific) for one hour. All debris and agents were removed by rinsing with water and the 1X PBS five times. All tissue was then dissected to remove larger, cartilaginous airways and cut into smaller chunks for processing. Processing of the decellularized tissue to achieve a fine powder included lyophilizing and freezer milling using a SPEX 6700. Powder was kept at -80° C until used put into electrospinning solution.

2.2.2 Scaffold Fabrication.

Scaffold was optimized by changing working distance, flow rate, needle size, and PLLA concentration. Resulting scaffolds were carbon coated and observed by Scanning Electron Microscope (SEM, Hitachi SU-70 FE-SEM). A final solution of 140mg of powdered PLECM was combined with 3 mL Hexafluoro-2-propanol (HFP) and mixed for 24 hours on a vortexer. 400 mg PLLA in 1 mL of HFP was mixed for the same period of time. The PLECM solution was poured into a syringe and pushed through a 150x150 mesh count stainless steel type 304 wire cloth into the PLLA solution to remove any large clumps of ECM that were not in solution. The mixture was then vortexed again for an hour to create the final PLLA/PLECM/HFP solution. Pure PLLA control solution was made by adding 400 mg PLLA to 4 mL of HFP and vortexed for one hour. Solutions with 35 mg and 0 mg PLECM with 100mg PLLA per mL HFP were electrospun onto a rectangular mandrel, 27 cm away from the needle and a rate of 4.5 mL/hr. 35 mg/mL PLECM solutions were electrospun with a voltage of 27kV and the PLLA only was electrospun with a voltage of 15kV, which were arrived at by the establishment of a stable Taylor cone.

2.3 Acellular Scaffold Characterization.

2.3.1 Scaffold Architecture

Scaffolds with various concentration of ECM were dried in a desiccator for a minimum of 24 hours before sputter coating for 60 seconds. Scaffolds were imaged with Scanning Electron Microscopy (SEM, Hitachi SU-70 FE-SEM) to show fiber size and architecture. Decellularized ECM tissue without processing was also sectioned and carbon coated after lyophilization for SEM imaging. Average fiber diameter and distribution of

the scaffolds were determined by taking measurements of 200 plus fibers per image, within three images of each scaffold type.

2.3.2 Mechanical testing

Elastic properties of PLLA scaffolds with varying amounts of PLECM (35 mg/mL and 0 mg/mL), with and without cells were tested using MTS Bionix 200 with TestWorks 4.0 Software, using established tensile testing protocols. Samples were taken from various scaffolds produced on different dates to cover batch to batch variability. Scaffolds without cells were wet for one week with Smooth Muscle Basal Media (SmBM, Lonza) to simulate physiological wet conditions. Scaffolds with cells were cultured for one week in a 24 well plate with dog bone shaped scaffolds held to the bottom of the wells with o-rings (Aflas). 50,000 HBSMCs (Lonza) were seeded onto each dog bone with Smooth Muscle Growth Media (SmGM, Lonza), changed every two days.

2.3.3 Contact Angle Measurement.

Wettability of the composite nanofiber mat was determined using the sessile drop method with an OCA 15 Goniometer with controlled automatic liquid deposition and a computer based image processing system. 5 µL of dH2O were deposited onto the fiber meshes with varying concentrations of PLECM. Each concentration type was repeated 4 times and the average contact angle was taken.

2.3.4 SDS-PAGE

SDS-page of scaffold proteins was performed to determine which ECM proteins and how much of each were present in the scaffolds post decellularization and electrospinning. 100 mg of intact tissue, 100 mg of decellularized tissue, and 200 mg of

each scaffold were put into a mixture of 1% SDS, 25 nM Tris, and 4.5 M Urea and heated to 60^0C for one hour, to increase the amount of protein re-suspended. The loading efficiency of DPLECM into the electrospun scaffold was determined using the final weight of the scaffold and ratio of PLLA and DPLECM in the solution before electrospinning. The yield of pure DPLECM within 200 mg of the 35 mg/mL PLECM/PLLA electrospun scaffold was the amount used for both DPLECM powder and DPLECM powder with HFP, to compare to the electrospun scaffold. The decellularized pig lung powder treated with HFP was allowed to fully evaporate after the HFP soak. Both were then put in 1 mL of the 1% SDS, 25 nM Tris, and 4.5 M Urea solution and heated to 60^0C for one hour. Protein concentration was measured using a Peirce™ BCA protein assay kit. All samples except PLLA, were balanced to the protein concentration of the 35 mg/mL PLECM/PLLA scaffold. 11.25 uL of 5 ug/uL protein and 3.75 uL of Laemmli buffer were loaded into each well of a 15 well, Mini-PROTEAN TGX stain-free gel (BIO-RAD) and run for 25 minutes in a Mini-PROTEAN tetra system (BIO-RAD) with running buffer. Resulting bands were imaged using a BIO-RAD gel imager.

2.3.5 Histology

Scaffolds were cryosectioned at 10 to 20 µm with a Thermo FSE Cryostat and stored frozen. Before staining, slides were heated to 100°C to increase specimen attachment. Sections of 35 mg/mL and PLLA only were stained with Masson's trichrome (Sigma) including hematoxylin (Sigma) following manufacturers protocol, to show ECM components. Imaging of ECM proteins within the scaffolds was done with the use of a light microscope.

2.3.6 Collagen and Elastin quantification

Elastin and collagen quantification procedure was taken from an established protocol [41]. 10 mg of electrospun scaffolds (PLLA and 35 mg/mL PLECM) and 10 mg of ECM powder were used for both quantifications. The samples and ECM powder were solubilized in 0.1 M NaOH at 98°C for 45 min. The supernatant was removed and lyophilized before hydrolyzing for 24 hours in 6M HCL at 110°C. The samples were lyophilized again and resuspended in 2 mL of DI water. For the collagen quantification all protein was put through a hydroxyproline assay (Sigma). For the elastin quantification, the same material samples were quantified with ninhydrin assay according to previously published methods [39]. Resulting data for ECM powder was normalized based on loading efficiency of the ECM into the polymer. ECM yield was found using the final weight of the scaffold and ratio of polymer to PLECM powder.

2.4 Cell Culture

2.4.1 Cell and media specifications.

Scaffolds and coatings were all sterilized with ethanol and rinsed with PBS before cultured with cells. HBSMCs (Lonza) were passaged continuously when confluency reached 80%. HBSMCs between passages 2-8 were expanded in SmGM (Lonza) with medium changed every 48 to 72 hours. All scaffolds were anchored to the bottom of tissue culture plates with Aflas-O Rings (24-well plates) or silicone (6-well plates, Loctite).

2.5 Cell Viability and Proliferation

2.5.2 Live/Dead Cell Viability Assay

HBSMCs were seeded at a density of 50,000 cells onto PLLA and 35 mg/mL PLECM/PLLA scaffolds at the bottom of a 24 well plate. After 72 hours in culture, reagents were added to label live cells (calcein AM, Thermo Fisher Scientific) and dead cells (Ethidium homodimer-1, Thermo Fisher Scientific) according to manufacturer's directions. After incubating in the reagent for 30-45 minutes the samples were mounted onto glass slides and imaged with an Olympus IX71 inverted microscope. Each scaffold type had three samples with three images taken of each sample. Live and dead images were combined and quantified using Image J analysis.

2.5.3 Qualitative SEM Imaging

200,000 HBSMCs were seeded onto 24-well sized scaffolds and cultured for one week. All samples were rinsed with PBS before fixing with 4% paraformaldehyde for a minimum of 20 minutes and rinsed again with PBS. After the initial fixation, the samples were put through secondary fixation with osmium tetroxide for one hour. To remove water, samples were ethanol dehydrated for critical point drying. The samples were dried using a Tousimis Critical point dryer, carbon coated for 60 seconds, and imaged using a JEOL JSM-5610LV SEM.

2.6 Cell phenotype

2.6.1 qPCR

Gene expression of 1,000,000 HBSMCs seeded onto scaffolds or coatings of various concentrations PLLA and PLECM for one week were quantified using qPCR. Cells and scaffolds were put into 1 mL of TRIzol (Life Technologies) and homogenized using 0.5 mm zirconium bead homogenization tubes and a microtube homogenizer

(Beadbug) and any remaining chunks of scaffold were removed. RNA was then extracted following Trizol manufactures protocol. RNA concentration and quality was quantified using a Take3 mircovolume plate (BioTek) and an Epoch reader. RNeasy kit (Qiagen) was then used to purify RNA if samples did not have a 260/280 ratio of 2 +/- .3. Using a high capacity cDNA reverse transcription kit (Applied Biosystems), balanced RNA was converted to cDNA. qPCR was run on CFX connect real-time system (BIO RAD) using powerSYBR Green PCR Master Mix (applied Biosystems). The expression of mRNA was determined by relative Cq value to zero. Four primers were used including α-SMA, CNN1. MYH11, and COL1 A1 (IDT). Primer sequences are listed in Table 1.

Primer	Gene	Forward Primer Sequence
α-SMA	Alpha Smooth Muscle Actin	5' CCG ACC GAA TGC AGA AGG A 3'
CNN1	Calponin 1	5' GTC AAC CCA AAA TTG GCA CCA 3'
MYH11	Myosin Heavy Chain 11	5' CGC CAA GAG ACT CGT CTG G 3'
COL1 A1	Collagen 1 A1	5' GTG CGA TGA CGT GAT CTG TGA 3'

Table 1: Primer sequences of contractile genes used in qPCR.

2.6.2 Immunofluorescence.

Scaffolds in a 24-well plate were seeded with 100,000 HBSMCs for one week. Scaffolds were fixed with 4% PFA and rinsed with PBS three times. To assess morphology and cell-cell connections, scaffolds with cells were stained FITC labeled phalloidin (Cell Signaling) according to manufacturer's protocol and imaged using a Zeiss LSM 710 Laser Scanning Microscope.

2.7 Statistics

Unless otherwise stated, GraphPad Prism was used for all statistical analysis. One-way ANOVA with Turkey pot-hoc comparisons or T-tests were done when appropriate to determine significance. Significance is represented by: *p-value < 0.05, **p-value < 0.01, ***p-value < 0.005.

CHAPTER 3: Results

3.1 Acellular Scaffold Characterization

3.1.1 Scaffold architecture

Fiber size and density were first optimized for smooth muscle cell sustainability by tayloring electrospinning parameters. Changes were made in flow rate (Figure 7-C), working distance (Figure 7-C,D), needle guage (Figure 7-E), and PLLA concentration (Figure 7-F) as compared to Regular 35 mg/mL PLECM (Figure 7-A) and PLLA (Figure 7-B). The most significant decrease in fiber diameter was seen when PLLA concentration was decreased. Any other strategy of changing fiber size did not seem to have any significant change in fiber size distribution as compared to scaffolds made from orginial electrospinning parameters.

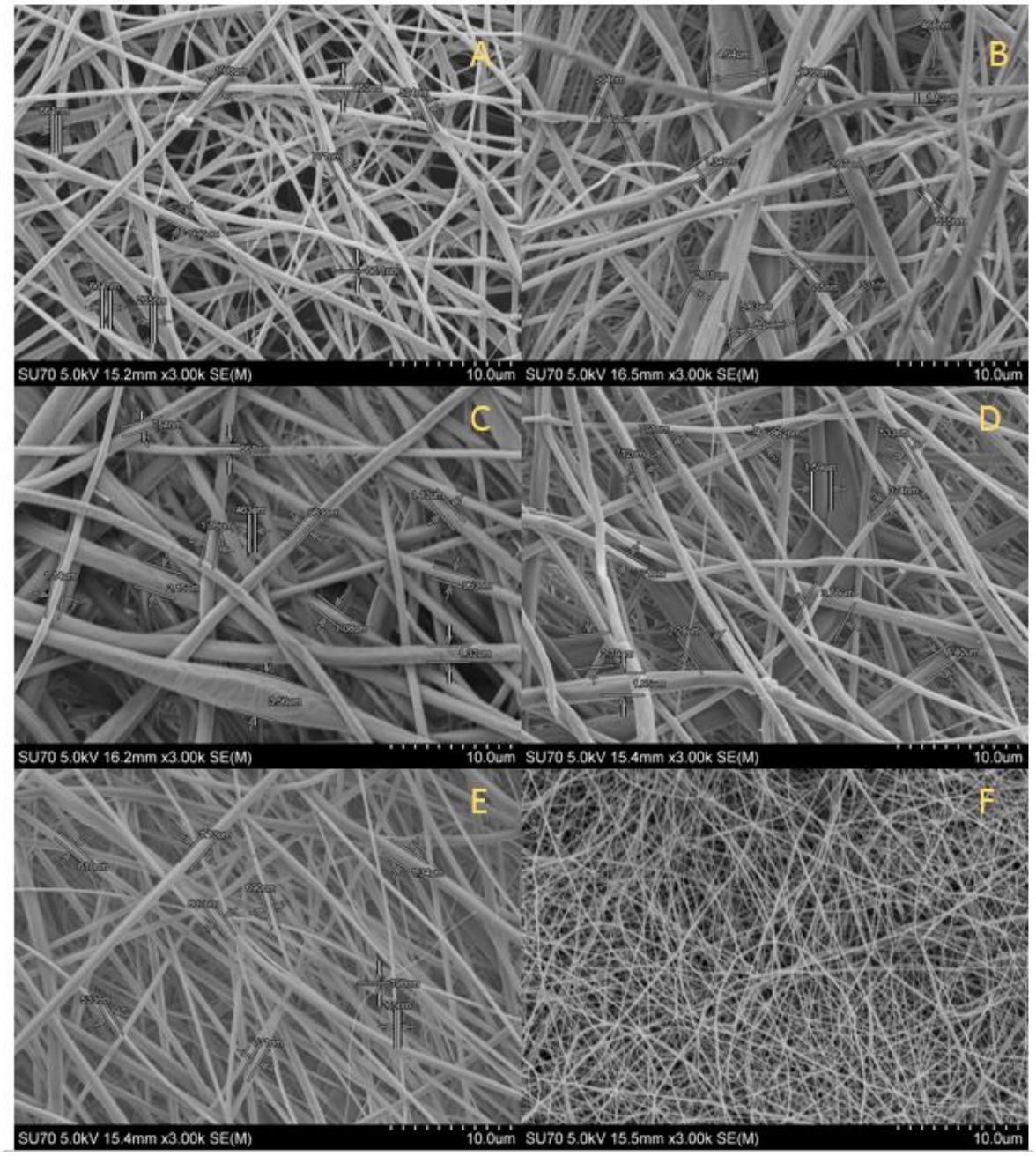

Figure 7: Changes in electrospinning parameter to optimieze fiber diameter. Regular 35 mg/mL PLECM (A) and PLLA (B) are compared to fiber diameter when flow rate was changed to 2 mL/hr instead of 4 mL/hour and working distance was changed to 15 cm instead of 27cm (C), when only working distance was changed to 6 inches instead of 27

cm (D), when needle guage was changed to 23G instead of 19G, and when PLLA concentration was decreased to 100 mg PLLA with 140 mg of PLECM instead of 400 mg PLLA with 140 mg of PLECM (F).

Optimized PLLA/PLECM scaffolds were imaged using SEM to examine the characteristics of the nanofibers. Electrospinning PLLA and PLLA/PLECM composite created a nanofibrous scaffold with the diameter and morphology shown in shown in Figure 8A-7D. Electrospinning with our optimized parameters created nanofibers similar to the size of the fibers of whole decellularized lung tissue seen in Figure 8E and 8F. The most uniform fibers in Figure 8E are seen in the regions where smooth muscle would most likely be located below the basement membrane of the airways, shown by the arrow.

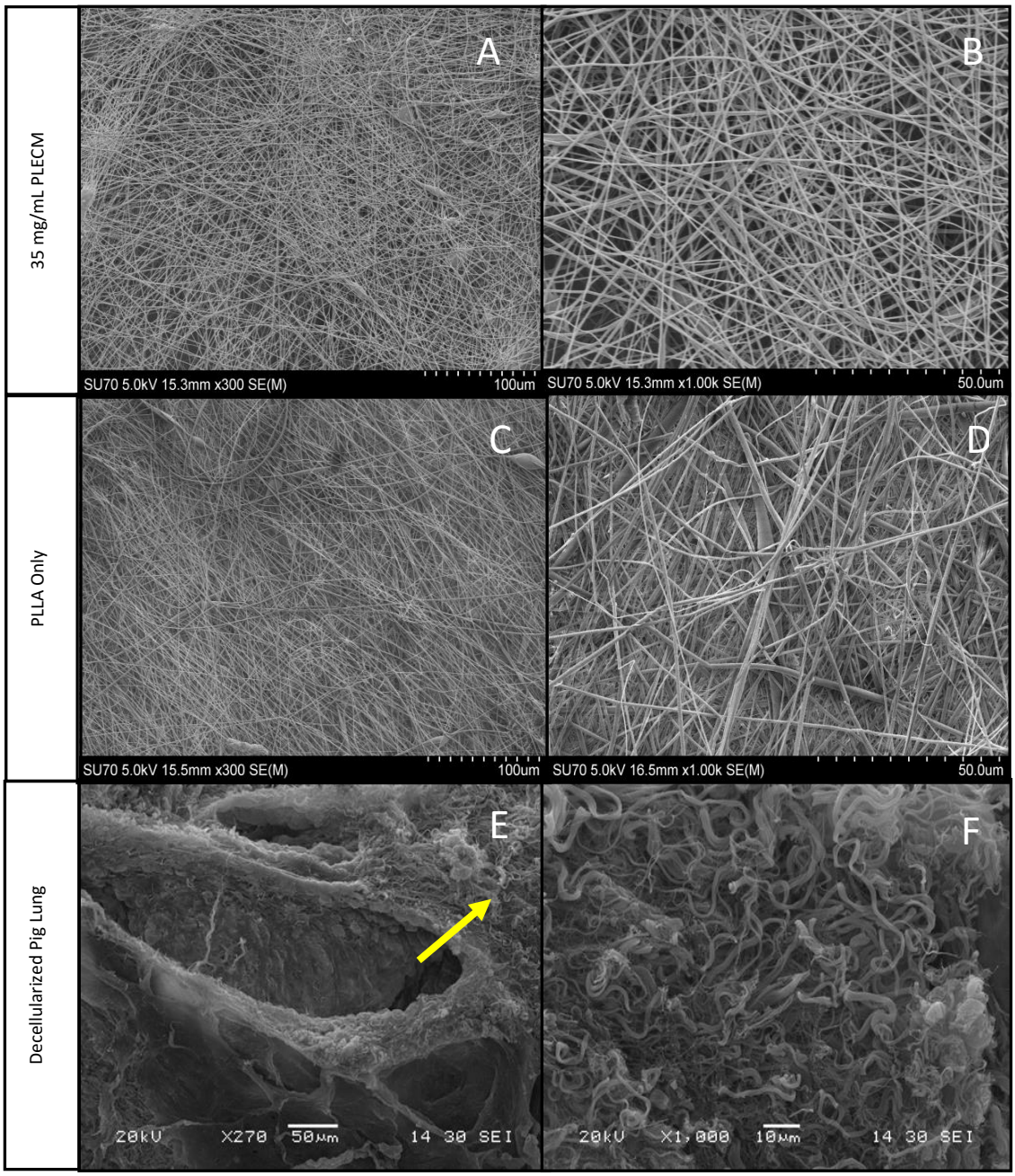

Figure 8: Scaffold and decellularized tissue fiber thickness. SEM of electrospun A-B) 35 mg/mL PLECM/PLLA and C-D) PLLA only scaffolds to compare to E-F) Decellularized ECM fibers that relate directly to natural fibers found in the airway environment.

Three SEM images were taken of each scaffold and from those images, 200 or more measurements of fiber width were taken. Average fiber thickness for PLLA only electrospun scaffolds was found to be 712.4 nm+/- 462.4 nm with a range from 54 nm to 4702.1 nm. 35 mg/mL electrospun scaffolds had an average fiber diameter of 806.4 nm +/- 432.1 nm with a range from 232.5 nm to 4783 nm as seen in Table 2. Average scaffold thickness was found to be of 139µm+/- 53µm. Fiber distribution (Figure 9) shows the majority of fibers to have a diameter from 250 nm to 750 nm.

	Average Diameter (nm)	STDEV (nm)	Min (nm)	Max (nm)
35 mg/mL	806.4	432.1	232.5	4783
PLLA only	712.4	462.4	54	4702.1

Table 2: Fiber diameter of electrospun scaffolds.

A) **35 mg/mL PLECM/PLLA Fiber Distribution**

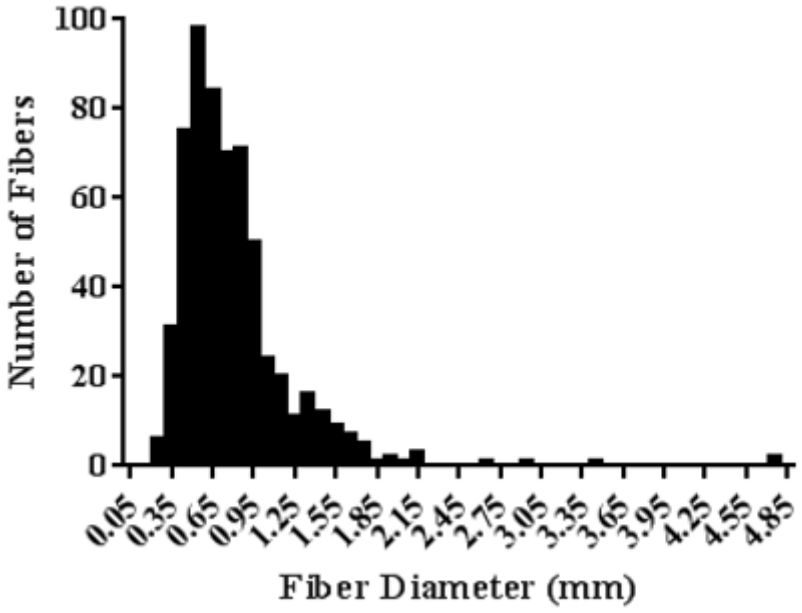

B) **PLLA only Fiber Distribution**

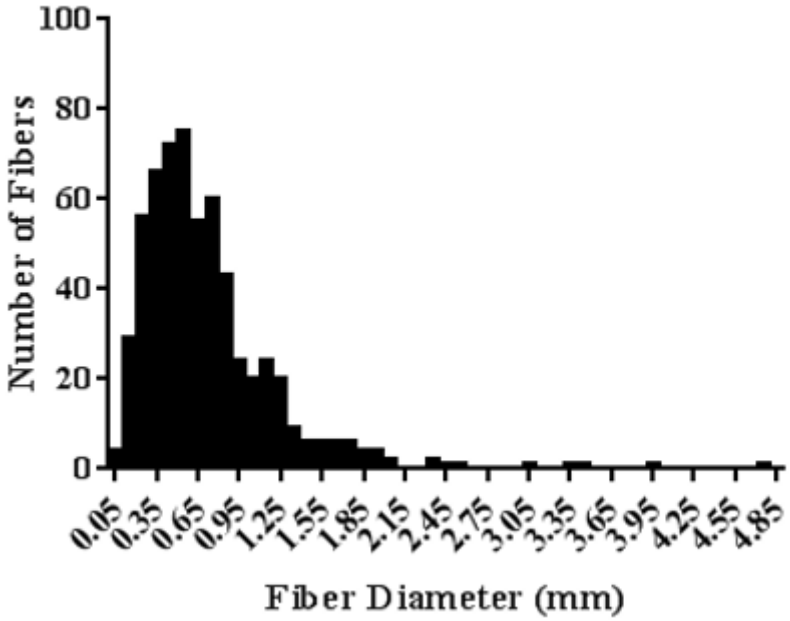

Figure 9: Fiber distribution of A) 35 mg/mL PLECM/PLLA and B) PLLA only electrospun scaffolds. Range and distribution taken from three images per group with 200 plus fiber measurements.

3.1.2 Mechanical testing

Uni-axial tensile testing of the PLLA scaffolds with various amounts of PLECM after a 1 week soak in basal media was done to determine several mechanical properties including elastic modulus, to compare to natural tissue. The addition of PLECM to the scaffolds decreased the average elastic modulus by 34.11 MPa. Both scaffolds were cultured with HBSMCs for one week to determine the amount of remodeling done to the scaffolds and its effect on the elastic modulus. Remodeling by the smooth muscle cells was found to have a significant effect on the properties of the scaffolds by decreasing the average PLLA scaffold modulus to 16.35 MPa and the ECM modulus to 14.03 MPa. It is important to note that many of the 35 mg/mL scaffolds with cells were too weak to be loaded into the MTS machine and therefore were untested. For that reason, the resulting data only represents the stiffest of the 35 mg/mL scaffolds with HBSMCs. Figure 10 compares scaffolds with various amounts of PLECM, with and without cells. Overall the addition of PLECM significantly decreased the mechanical properties of scaffolds with and without cell intervention to more closely mimic the properties of natural tissue as expected.

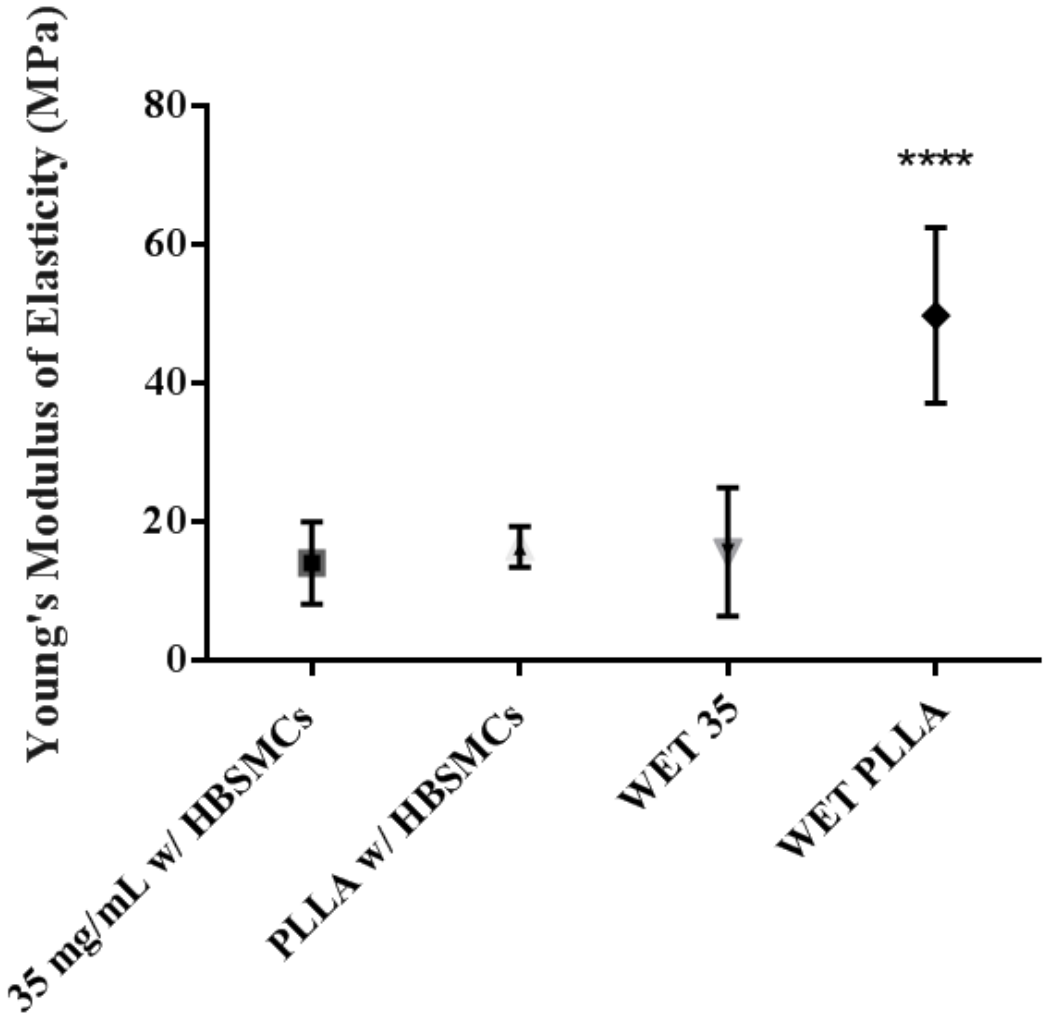

Figure 10: Elastic modulus of electrospun scaffolds. Tensile testing for scaffolds with various amounts of PLECM under wet conditions, with and without cells. 35 mg/mL w/ HBSMCs and PLLA w/ HBSMCS represent respective scaffolds with HBSMCs cultured for one week. Wet 35 and wet PLLA represent scaffolds that have been soaked in media for one week without cells. Data are presented as mean +/- st. dev. Sample size varied between 4 and 11 per group. 4 of 11 samples show for 35 mg/mL with HBSMCs because

of scaffold weakness making some samples untestable. PLLA was significantly greater to all other groups. **** $p<0.0001$

3.1.3 Contact Angle Measurement.

Average results of the resulting water contact angle of a 5µL dH2O drop on the 35 mg/mL PLECM and PLLA nanofiber composite scaffold and PLLA only scaffold with the sessile drop method are shown in Figure 11 and Table 3. Overall the water contact angle decreased with increasing PLECM with an average decrease of 14.1° between PLLA only and 35 mg/mL PLECM.

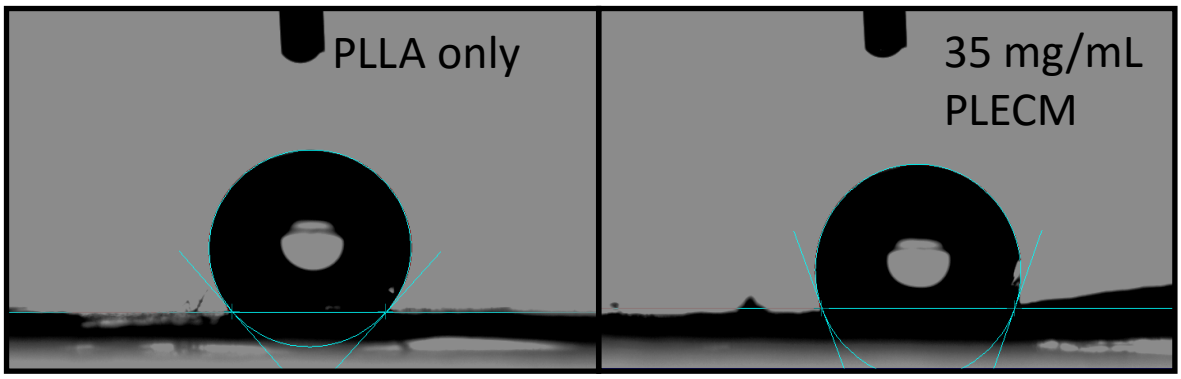

Figure 11: Contact angle measurements on electrospun scaffolds.

	Average Contact Angle	Number of Samples
35 mg/mL PLECM	115.1° +/- 3.5°	4
PLLA only	129.2° +/- 1.9°	4

Table 3: Contact angle measurements of various electrospun scaffolds.

3.1.4 SDS-PAGE

SDS-PAGE was performed on protein extracted from intact pig lungs, decellularized pig lungs, decellularized pig lung powder, decellularized pig lung powder in HFP, and scaffolds containing only PLLA and 35 mg/mL PLECM/PLLA, shown in Figure 12. PLLA was a control to show effects of the polymer alone. The differences between decellularized ECM powder and the 35 mg/mL scaffolds highlights the effect that electrospinning and the harsh solvents used for electrospinning have on the integrity and existence of ECM proteins. Intact tissue has a wide range of proteins resulting in many bands, while decellularized tissue has fewer protein bands due to the removal of cells and blood that contribute to the vast assortment of proteins. Powdered DPLECM and Powdered DPLECM in HFP have similar bands at 25 and 15 kDa but treating with HFP causes many larger proteins to be lost or degraded to a smaller protein fragment. A similar amount of bands are present in the pure DPLECM powder in HFP and the 35mg/mL PLECM scaffold with the exception of a few bands. These results showed no significant bands of protein present from PLLA, as expected.

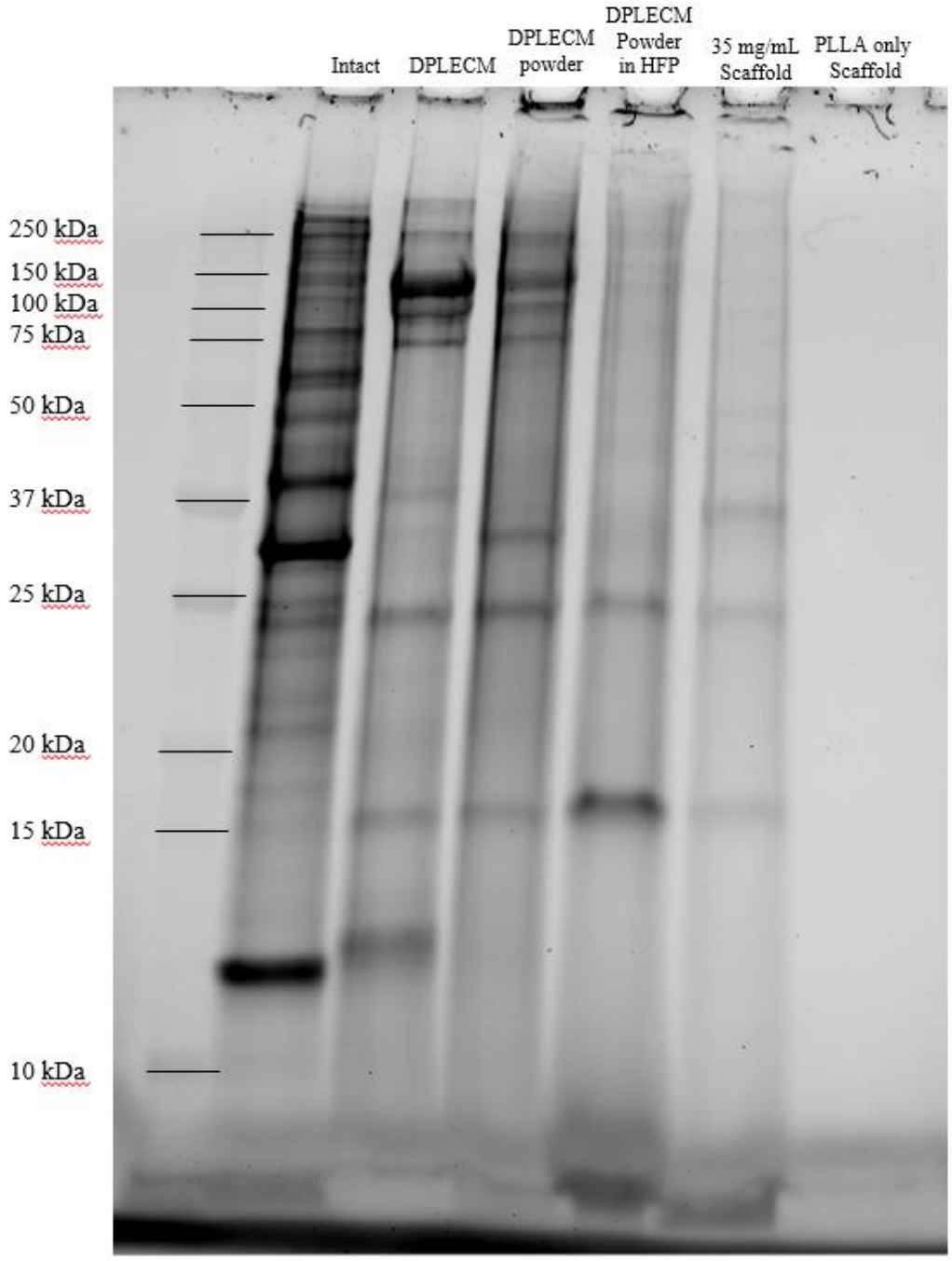

Figure 12: SDS-PAGE of electrospun scaffolds vs. intact pig lungs, DPLECM, and DPLECM powder.

3.1.5 Histology

Sections were taken from the various scaffolds using cryosectioning and stained with Masson's Trichrome ECM protein dye. PLLA was used as a control containing no ECM proteins but also further demonstrated the regularity of the nanofiber structure throughout the scaffolds. After staining 35 mg/mL scaffolds there was prominent amounts of collagen, stained purple, and elastin, stained black (Figure 13). While imaging there was a large amount of light refracting, causing images to be more distorted than usual. The proteins are dispersed throughout the PLECM/PLLA scaffold, with purple showing collagen and black showing elastin. The dark purple and black dye is seen throughout the scaffold as well as throughout the fiber. Large spots of stained scaffold are likely sectioning artifacts, which are confirmed by the absence of these structures in previously shown SEM images of scaffolds.

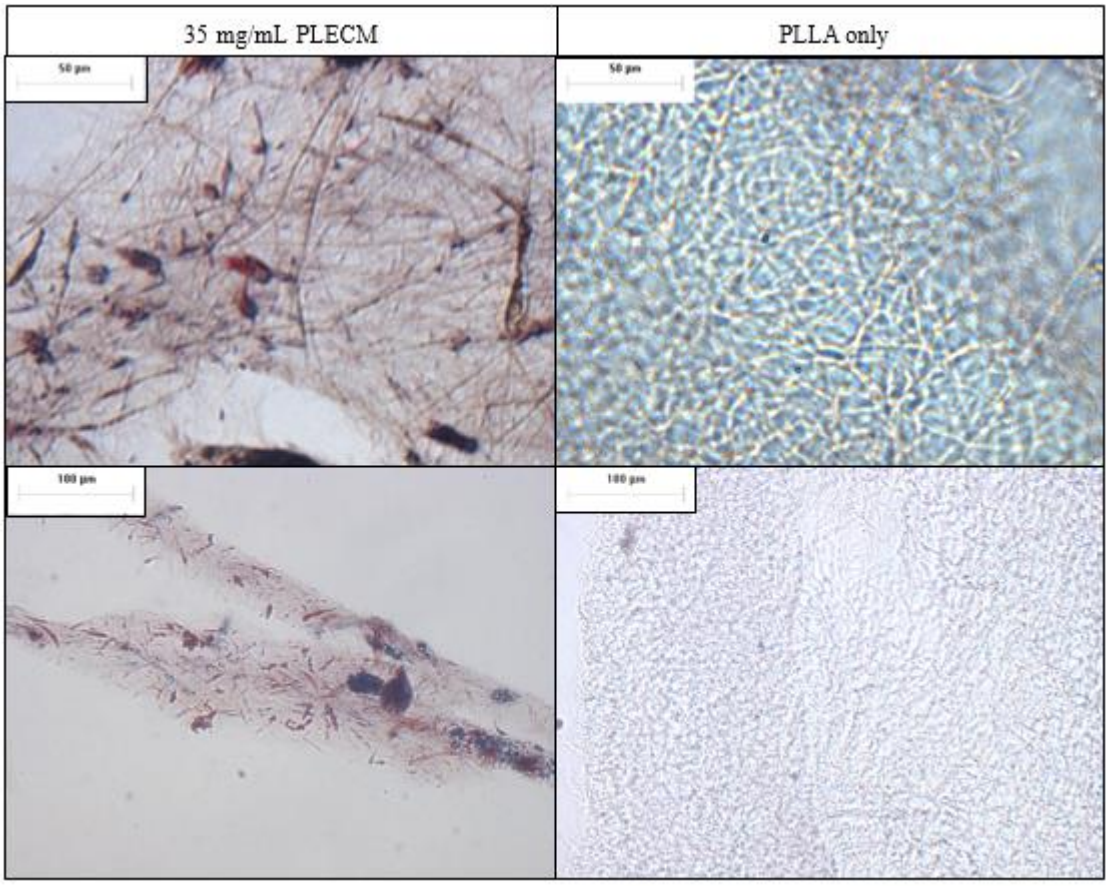

Figure 13: Masson's trichrome staining of electrospun scaffolds to confirm presence of ECM protiens in PLECM scaffold vs. PLLA only scaffold.

3.1.6 Collagen and Elastin Quantification

Collagen and elastin were quantified with hydroxyproline and ninhydrin assays respectively, to determine the amount of the essential ECM proteins were in the scaffolds after electrospinning. Scaffolds were normalized with PLLA values that accounted for background. The amount of pure ECM powder within the 10 mg of scaffold was determined and used as a comparison. A large amount of collagen was found in the PLECM electrospun scaffolds but significantly less than seen in pure ECM. Elastin

amounts were determined using an amino acid quantification assay and showed more elastin content in the scaffolds than in pure ECM powder.

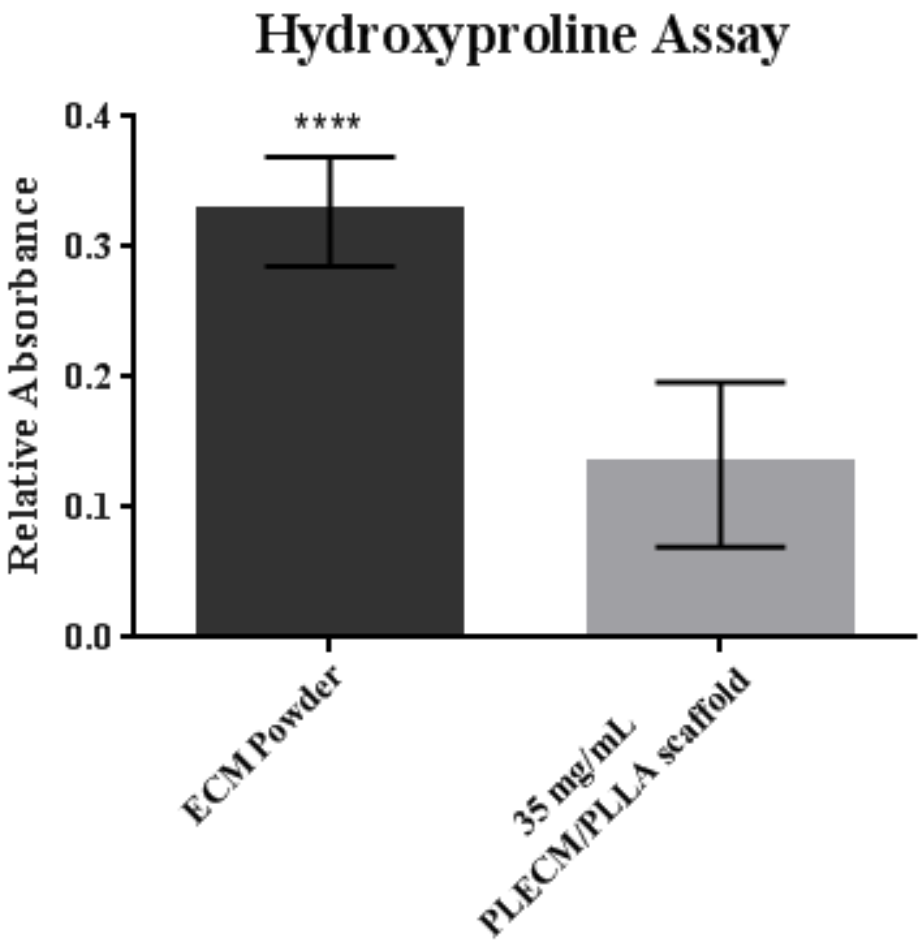

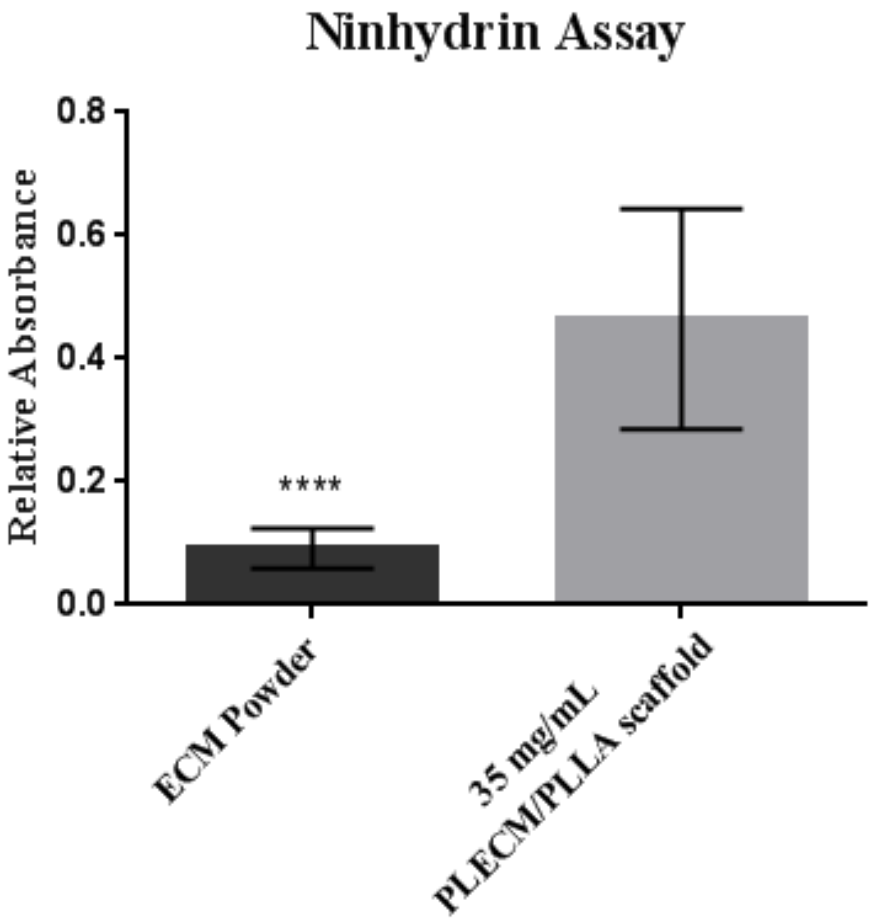

Figure 14: Collagen content shown by hydroxyproline quantification and elastin content shown by ninhydrin assay with electrospun scaffolds. Values normalized to PLLA background. Data are presented as mean +/- st. dev. Sample size varied between 9 and 17 per group. **** $p<0.0001$

3.2 Cell Viability and Proliferation

3.2.1 Live/Dead Cell Viability Assay

Live/Dead florescence imaging show a large amount of live (green) cells on both scaffolds but a significant many more dead (red) cells on the PLLA scaffolds (Figure 15).

There is also a difference between cell morphology on the two different scaffolds. Many more cells on the PLLA have a circular morphology and those that have extending appendages, have much smaller area coverage and extension. Quantification of several samples per group (Table 4) showed a consistent increase in dead cells on PLLA samples as compared to 35 mg/mL samples.

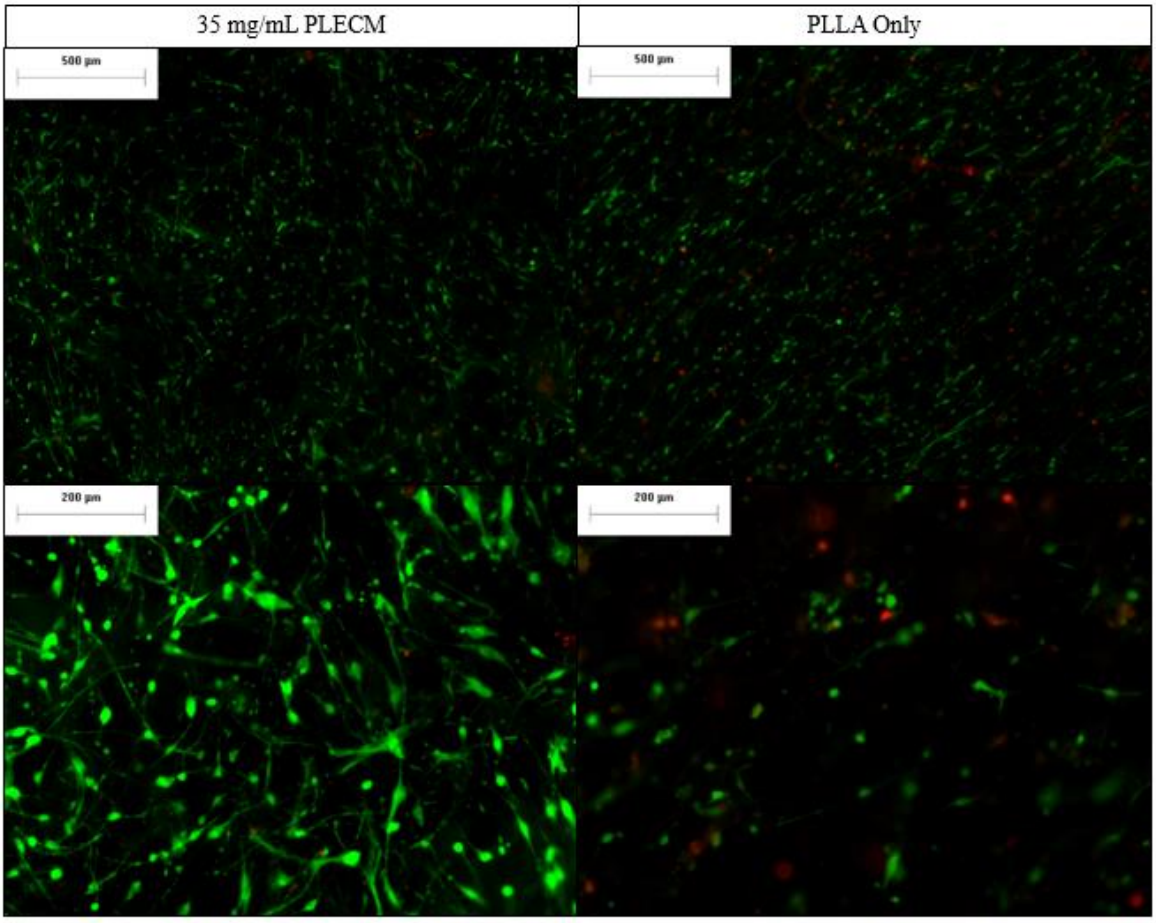

Figure 15: Live/Dead imaging of HBSMCs on scaffolds. Live cells are stained green and dead cells are stained red. Sample size of 3 with at least 3 images taken of each sample.

	Average % Dead	Average % Live
35 mg/mL PLECM	0.34 +/- 0.22	99.66 +/- 0.22
PLLA only	13.29 +/-11.95	86.71 +/- 11.95

Table 4: Quantification of Live/Dead images. Average +/- st. dev. Averages taken from 9 to 11 images per group.

3.2.2 Qualitative SEM Imaging

SEM of HBSMCs on scaffolds cultured for 1 week show a significant amount of cell attachment and cell spreading on both scaffolds (Figure 16). There are qualitative differences in morphology and spreading between the scaffolds with PLECM and scaffolds without PLECM. Cells on the 35 mg/mL scaffold show confluent layering than those on PLLA only scaffolds.

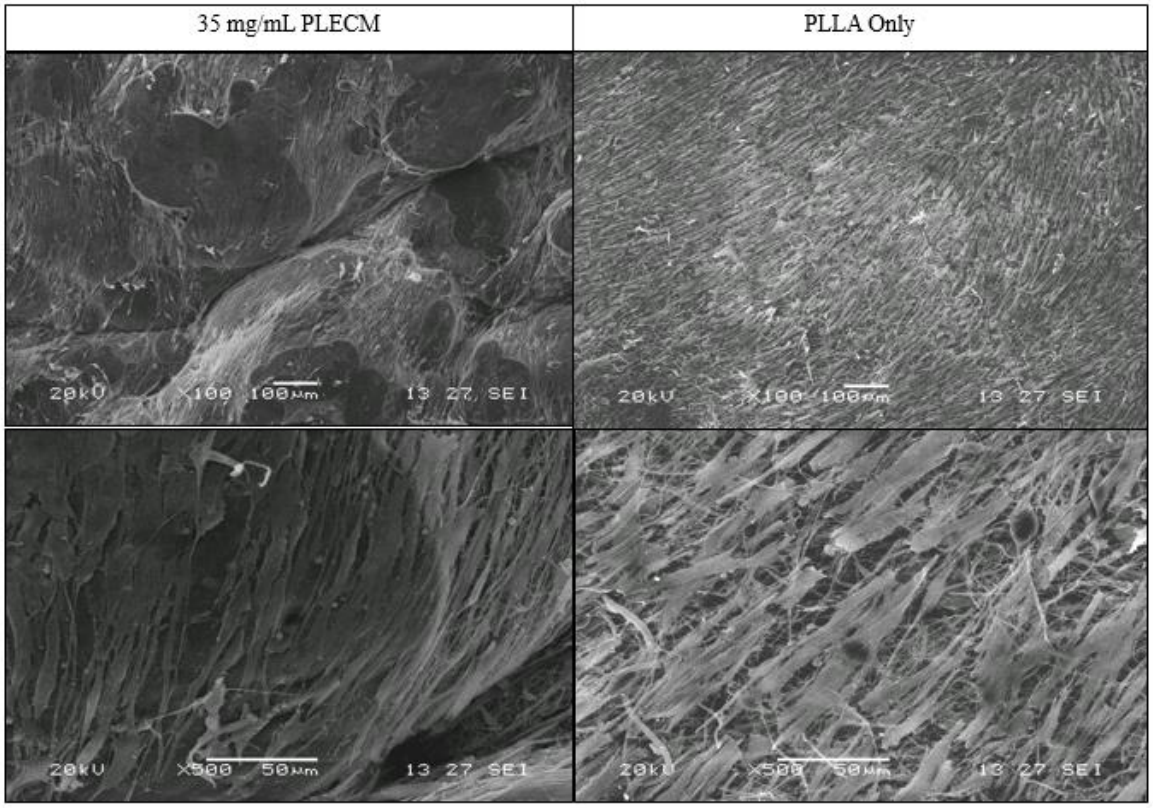

Figure 16: SEM of HBSMCs on scaffolds. Week long culture of cells on scaffolds showing morphology and cell attachment.

3.3 Cell phenotype

3.3.1 qPCR

To evaluate the impact that PLECM and electrospinning had on gene expression of contractile proteins and ECM production proteins, gene analysis was run alpha smooth muscle actin (αSMA), calponin 1 (CNN1), myosin heavy chain 11 (MYH11), and collagen 1 (COL1 A1) with relative Cq values seen in Figure 17. All values are absolute data and are not relative to any housekeeping genes. In all cases, except for myosin heavy chain 11 expression, HBSMCs on both types of electrospun scaffolds had increased expression over

PLLA and 35 mg/mL PLECM coatings. Similar expressions of αSMA were seen between PLLA and 35 mg/mL PLECM scaffolds but there seemed to be an increase in expression for the PLLA coating compared to the 35 mg/mL PLECM coating. In the case of CNN1, PLLA coatings and scaffolds showed more expression than their 35 mg/mL PLECM counterparts. Cells on scaffolds expressed less MYH11 than cells on both coatings but cells on PLLA coatings expressed more MYH11 than 35 mg/mL PLECM. A large increase was seen in the expression of COL1 A1 by cells on 35 mg/mL PLECM electrospun scaffold compared to PLLA only electrospun scaffolds.

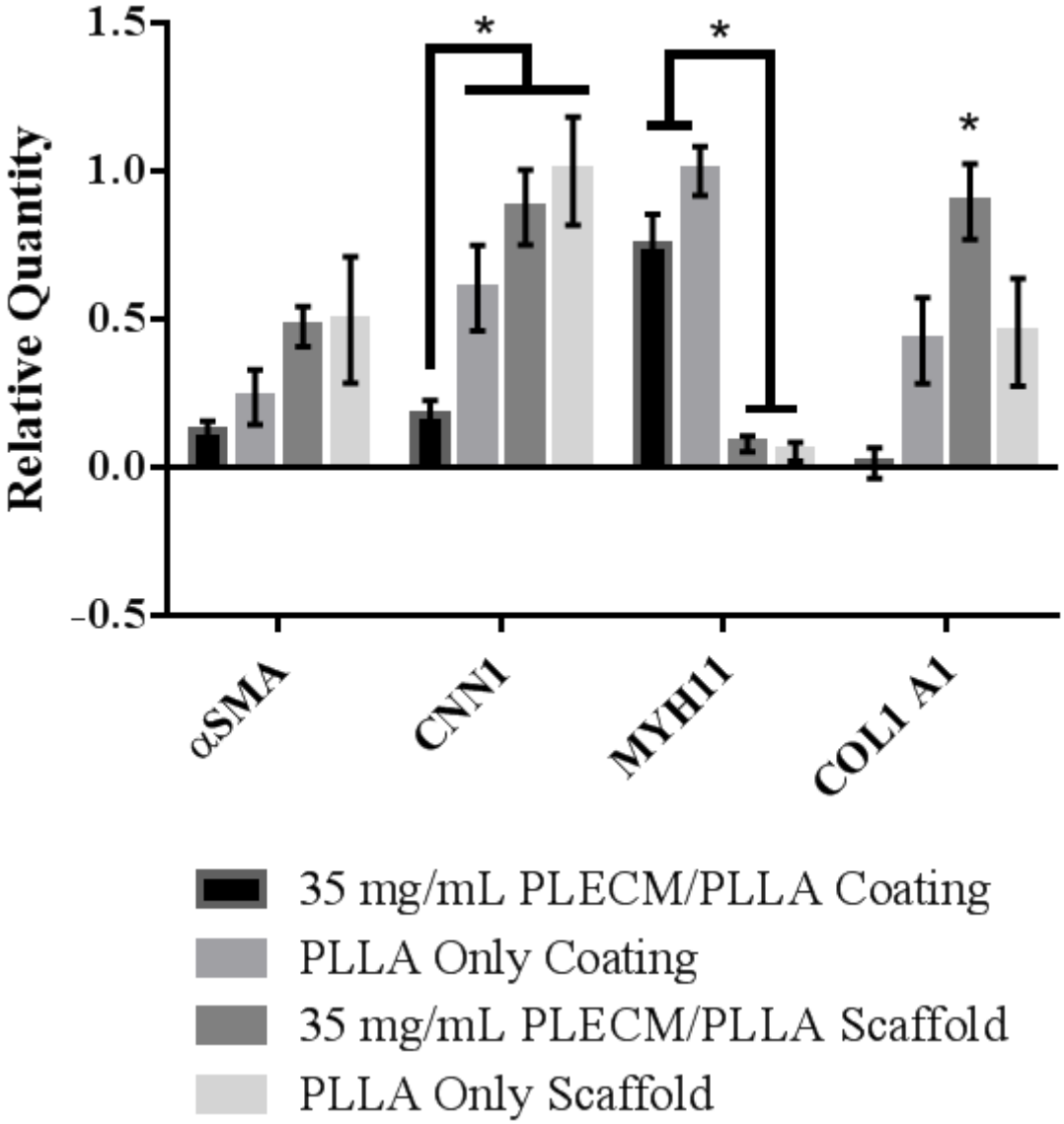

Figure 17. qPCR data of HBSMCs on scaffolds and coatings for one week. Values shown are relative Cq values. Data are presented as mean +/- st. dev. Sample size varied between 3 and 4 per group. Significance was defined as * $p < 0.05$ as indicated.

3.3.2 Immunofluorescence.

Phalloidin staining of F-actin in HBSMCs on PLLA and 35 mg/mL scaffolds in Figure 18 showed a large amount of cells attaching to both scaffolds, but there are also differences in morphology and actin distribution between the two different scaffolds. Cells on 35 mg/mL show a more spread out morphology with many projections with dense actin filaments. PLLA, in comparison has much less cell spreading with many cells still circular in morphology and only one to two projections per cell. Cells on PLLA also have actin filament staining mostly located centrally in the cell.

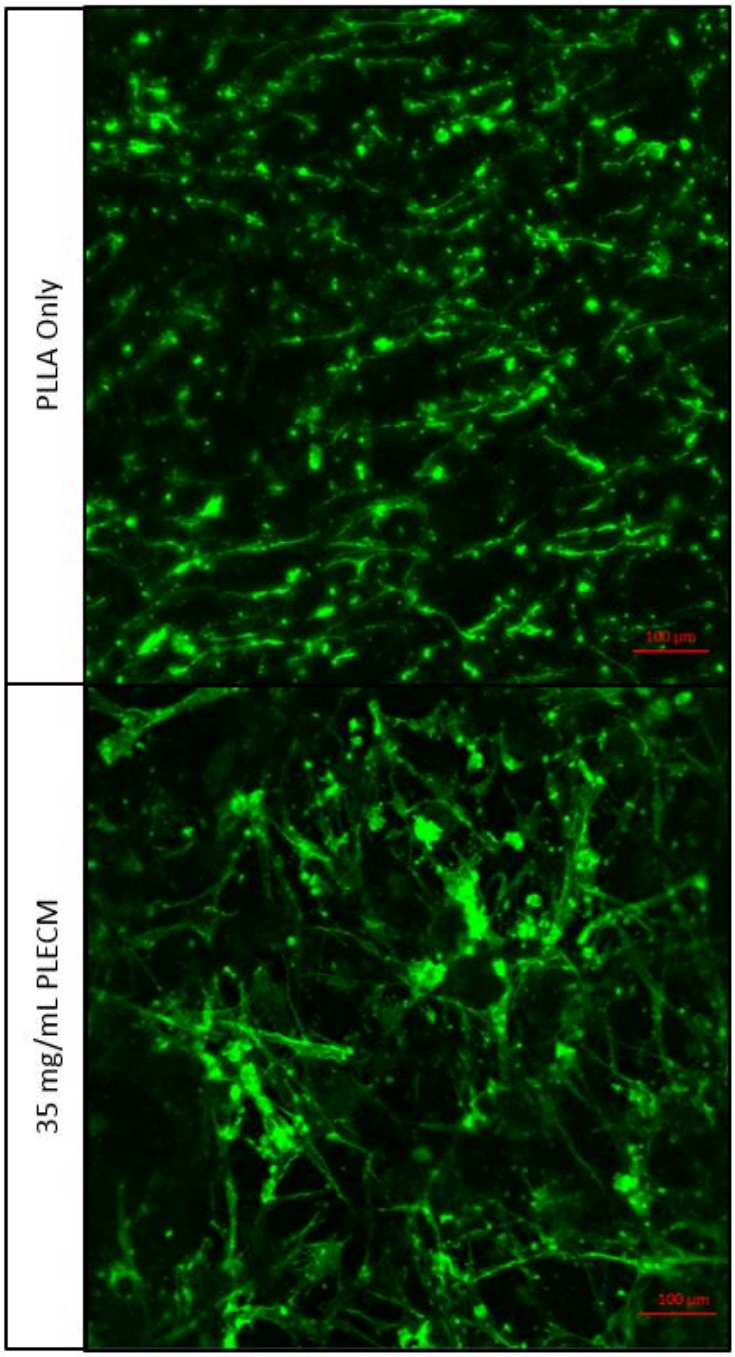

Figure 18: F-actin immunofluorescence staining of HBSMCs on scaffolds. Green (phalloidin) staining shows localization of F-actin throughout the cells on PLLA and 35mg/mL scaffolds.

CHAPTER 4: Discussion

Overall there is a consensus within the literature that natural ECM environments with a detailed architecture are vital for properly modeling an ASM environment. Past approaches have limitations preventing the replication of a full model with mechanical and biochemical relevance. In order to develop an *in vitro* model of airway smooth muscle that has superior biomimicry of the natural bronchial tissue, the major objective was to develop a biosynthetic scaffold with strength and ECM protein composition. More specifically, our goals were to develop an electrospun scaffold consisting of a synthetic polymer and pig lung extracellular matrix (PLECM), verify the presence of key ECM components post-solublization and post-electrospinning, and finally investigate whether the scaffold can support SMC growth and maintain the smooth muscle contractile phenotype. The results led to the development of a novel nanofibrous mat on which HASMCs were able to grow and interact with the essential ECM proteins. ECM concentration and electrospinning parameters are critical for the structural and bioactive properties held by the scaffold. This is important because fibers resembling natural small airway ECM in size and composition directly effects cell phenotype. We can use decellularized airway tissue as a guide for scaffold topographies ranging in porosity and fiber density for each region. To ensure the smooth muscle cell interactions are physiologic, natural cell microenvironments for each cell type must be present with nano to micro sized fibers that provide the ability for cell alignment, directing smooth muscle cell growth in the circumferential direction around the airway for constriction purposes [35]. This data demonstrates the potential the

PLLA/PLECM electrospun scaffold has as a novel and superior *in vitro* model for the study of normal SMC interactions, disease modeling, or drug delivery research.

Current in vitro models of lung cellular environments using polymeric scaffolds do not fully represent the in vivo tissue environment. Studies done with fully synthetic polymers lack the natural ECM components needed for proper signaling with lung cells [42]. By adding the processing technique of electrospinning to polymers, it can offer many benefits of structural recognition [36] but lack biological signaling for proper physiological mimicking. Electrospinning of natural ECM elements to increase bioactivity has been extensively researched but most have only one or two ECM components represented [29], [30]. These engineered scaffolds have drawbacks because of the lack of a wide range of ECM components at a specific ratio present in organ specific decellularized tissue [22]. Other subpar *in vitro* models also struggle with the inability to retain growth factors, giving an incomplete representation of airway in vivo ECM environments [38]. A large amount of information is hidden in signaling molecules and binding sites within the extracellular environment that combine to form a unified complex picture that can only maintain tissue specific differentiation with all of the signaling players [43], [44]. Decellularized materials without further processing can also pose limitations because of uncontrollable shape, mechanical properties, and degradation rates. Developing a platform that permits the culturing of SMCs for the accurate testing of therapeutic and toxicity responses to drugs will open the doors to more effective drug testing and understanding of the natural cell/ECM interaction in diseased or normal states. In this study, we have designed a platform with these qualities by combining the tailorable structural support of PLLA with

sufficient ECM components for optimized cell attachment and tissue specific signaling [26].

The PLECM/PLLA scaffolds were successfully developed from decellularized pig lung [40] dissolved into HFP to allow for evaporation of the solvent during the electrospinning process. HFP was chosen because of its use in various prior studies [45]. Its boiling point of 61 degrees makes it prone to evaporation, a characteristic that is essential for electrospinning and having dry fibers as a final product [30]. This electrospun mixture allows for an increase of mechanical strength, control of ECM component release [37], and electrospinning consistency as compared to ECM alone. ECM concentration was chosen based upon a previously published collagen electrospinning protocol also using HFP [30] that showed concentration dependence associated with fiber diameter. Similar concentrations were used with minor modifications in electric potential based on the formation of a Taylor cone with the selected materials and quality of the final scaffolds. After optimization, the resulting concentration was determined to be 17.5 mg/mL and 35 mg/mL to give a mostly uniform nonwoven fibrous mat based on electrospinning properties alone. After further investigation, we saw in increase in the cell viability and attachment with the higher concentration of 35 mg/mL leading us to eliminate 17.5 mg/mL as an optimal concentration and removing it from all experiments.

We then moved on to optimizing properties for the culture of smooth muscle cells. The goal was to have a randomized fiber arangment of medium sized fibers resembling those found in the smooth muscle layer of airway wall, shown in figure 8E. The scaffold created by electrospinning the solution at 27 cm with a 4.5 ml/hr flow rate, and 19G needle

produced the most desirable fiber diameter. Looking closer into the region of the airway where smooth muscle is found in the lung figure 8F, fiber distribution is similar to what we have created with a difference in fiber shape. Natural ECM fibers have a coiled appearance when cut leading us to believe that fibers are naturaly under tension. Future investigations would be to construct fibers resembling the decellularized ECM by fabricating fibers under tension.

Another future investigation would be to achieve smaller fiber diameter scaffolds to optimized growth for epithelial cells. The most significant decrease in fiber diameter was seen when PLLA concentration was decreased. While this seemed encouraging, we were unsure about the quality of this scaffold because there seemed to be issues with the PLECM stopping up the syringe. We concluded that the smaller fiber diameter was caused by a decrease in the available opening for PLLA to exit while the PLECM was clogging the syringe. Additional troubleshooting and investigating of the scaffold developed from the lower concentration of PLLA will need to be done in the future to see if this is a viable option for multicellular culture. If this could be achieved, our hopes would be to form a biphasic scaffold [35] in the future.

The most abundant ECM proteins in the lungs are collagen, mostly collagen type I, III, IV, and V, and elastin [30], [46]. The majority of the proteins just mentioned have a slightly larger nanometer sized fiber, causing cells to be accustomed to recognizing the majority of larger fibers and less of smaller fibers such as fibronectin, laminin, and other less frequent constituents. Many studies stress the importance of a distribution of nanofiber diameter that closely resembles the distribution in the specific anatomical ECM being

modeled [30]. Cells have the ability to recognize varying levels of protein structures, including, collagen fibrils ranging from 260 and 410 nm [47], elastin filaments from 3-4nm [48], elastin fibrils from 200 and 3000 nm [49], and smaller collagen fibers of just 50nm (collagen type 1, 4). With the use of SEM, it was confirmed that the electrospinning parameters chosen for specific concentrations of PLECM generated nano to micro-sized fibers with an average fiber size of 793.7 nm, similar to a collagen fibril or elastin fibril. The range of fiber sizes varied from 54 nm to 4702.1 nm with a much higher occurrence between 250 nm and 750 nm. With this fiber distribution the cells are experiencing the structural signals from all fiber sizes resembling all ECM proteins but with a much higher presence of collagen like fibers as is seen in the natural lung tissue where 90% of the dry weight is collagen [38].

Incorporating ECM proteins into synthetic scaffolds not only disrupts the mechanical strength of the synthetic polymer, but since the DPLECM already possess a similar modulus to natural tissue, it counteracts the high modulus of PLLA. Research has strongly supported the idea that tissue engineering scaffolds must possess mechanical characteristics matching the natural tissue to avoid failure or disruption of natural processes [50]. In an environment as dynamic as the lungs, cells sense the response of the surrounding ECM to mechanical loads spatially and temporally for the maintenance of natural signaling cascades and phenotype. Decrease of the scaffolds average elastic moduli by 34.11 MPa with the addition of PLECM, partially returns the scaffold towards the realm of intact lung tissue possessing a modulus of 0.5 kPa [51]. According to what is known about mechanical characteristics of decellularized and whole lung tissue, this value is what

should be expected for small airway scaffolds because the addition and remodeling of cells should then greatly decrease scaffold stiffness even further.

Addition of cells to our scaffolds for one week decreased the modulus of PLLA to 16.53. Naturally, the decrease in elastic modulus by remodeling would be caused by matrix metalloproteinases (MMPs) [52]. The breakdown of the PLLA fibers by these enzymes is questionable because of the lack of cleavage sites within the synthetic polymer. It is evident that there has been some breakdown to the PLLA structure, seen by decreased elastic modulus, but this could have been caused by a decrease in pH within the media from cellular metabolic waste. Evidence from gene expression of collagen 1 does support the theory that remodeling is still occurring but the breakdown of the fibers by the HBSMCs may not be taking place. It is also important to note that *in vivo* there would be an increase in the elastic modulus caused by ECM production. This is not seen here because the collagen and other ECM proteins that are being produced are not cross-linked because of the absence of Vitamin C. In the future, addition of vitamin C to the culture would be needed to see the true effect of remodeling by the cells. The same situation may be occurring within the 35 mg/mL scaffolds because of the PLLA within them but there is a presence of natural ECM components and their cleavage sites that would allow for some MMP breakdown. However, the data showed that when cells were cultured on 35 mg/mL scaffolds (14.03 MPa), the modulus did not change much from the 35 mg/mL scaffolds without cells. The insignificant change from 35 mg/mL scaffolds without cells to the 35 mg/mL scaffolds with cells was caused by the exclusion of many samples because they

were too weak to be loaded into the MTS machine. Future studies will include more precise measures of mechanical properties.

Since there were no problems loading the PLLA scaffolds with cells or the few thicker 35mg/mL scaffolds, it can be concluded that 35 mg/mL scaffolds may have an elastic modulus well below 16.35 MPa and therefore may have a much closer mechanical strength to natural lung tissue. We predict that with extended culture periods there will be more remodeling as more of the polymer is replaced with ECM produced by the ASM cells. The results showed PLLA only scaffolds also having beneficial remodeling with a significantly lower the average modulus to 16.35 MPa, but PLECM scaffolds started out at a more realistic modulus allowing it to take less cellular remodeling to reach the natural mechanical properties. By having a model that more accurately resembles the mechanical properties, the scaffolds will encourage realistic ECM deposition by the HBSMCs and maintain cellular phenotypic responses. The results showed that the addition of the PLECM not only improved the mechanical properties but also the physical hydrophilicity of the scaffold. Similar studies done with electrospinning bone ECM have shown that as more ECM is introduced into a composite, the less hydrophobic the scaffold will become [37] because the ECM is hydrophilic which induces cell attachment and proliferation [53].

Delving further into ECM scaffolds ability to increase attachment and behave accurately as an *in vitro* model, the question is, are all of the ECM proteins intact, prevalent, and recognizable post electrospinning? There is some concern about ECM proteins polymerizing with the PLLA during the electrospinning process, leaving binding sites and full proteins unnoticeable to the cells. Our research has found that after the

decellularization process there is still the presence of several smaller fragments of larger ECM components and possibly whole ECM proteins, just as was seen in other studies using this same decellularization procedure [40]. The data also determined whether the harsh solvent or electrospinning process causes any damage or masking of key proteins attachment sites or growth factors. Intact and decellularized tissue was used as a comparison to the amount of ECM components lost in the liquid nitrogen milling, HFP treatment, and electrospinning. Comparing samples treated with HFP to the DPLECM and DPLECM powder, there are significantly less bands after exposure to HFP because of HFP's ability to denture, open, and break apart proteins. There is much less difference in the amount of bands between the DPLECM powder in HFP and 35 mg/mL, allowing us to conclude that the process of electrospinning causes little effect to ECM proteins. There are still detectable amounts of proteins, either fragments or full, within the PLECM/PLLA electrospun scaffold that can offer various natural signaling cascades for the maintenance of smooth muscle phenotype. In summary, HFP denatures and unfolds proteins as compared to decellularized tissue and powder, but the resulting fragments of larger proteins are detectable after electrospinning. In future experiments, blotting the gels and probing with antibodies to membranes will allow for identification of specific ECM proteins.

With collagen and elastin being the most abundant proteins within the ECM [46], confirmation of these proteins in our scaffold is vital to determining the level of recognition the cells have with our scaffolds. Hydroxyproline and ninhydrin assays, which were performed to quantify both collagen and elastin, respectively, prove that there is a

significant amount of collagen and elastin in PLECM scaffolds. Collagen quantifications showed a decrease in collagen content as compared to ECM powder due to loss of collagen during the electrospinning process. Elastin, in contrast, was more prevalent in the electrospun scaffold than in pure ECM powder. This could have been caused by the electrospinning properties of elastin, such as charge or molecular weight that would ensure there is a large yield of elastin compared to other ECM proteins. Another possibility for this result could be the quantification method of detecting amino acids. There may have been a difference in the breakdown of the scaffolds and the ECM powder into amino acids. We do expect that most of the collagen and elastin quantified here would be broken down versions of these proteins because of the lack of banding for the electrospin scaffolds within the SDS-PAGE where collagen (200 kD) and elastin (81 kD) would be found.

The presence of these key ECM proteins was further confirmed by Masson's trichrome staining of ECM confirming the presence of collagen and elastin throughout 35mg/mL scaffold. Large clumps of scaffold with significant ECM staining are seen throughout the images but we have concluded that these are sectioning artifacts based on their absence in all other imaging of the scaffolds such as SEM. Staining offered us a more in depth look into the location and amount of the ECM proteins throughout the scaffold and fiber. Having well dispersed proteins throughout the fiber shows there will be an even released of proteins during degradation as well as randomized disbursement throughout the fiber for cell attachment. Our ECM stained histology, SDS-PAGE, and elastin and collagen quantification showed that we do have ECM components detectable within the scaffolds post-fabrication.

Following the characterization of the PLLA/PLECM scaffold and the confirmation of recognizable ECM proteins, the second objective of this research was to investigate the scaffolds ability to support growth, increase attachment, and differentiation of primary human bronchial smooth muscle cells. Previous studies using decellularized ECM have shown increased cell adhesion and proliferation in the case of urinary bladder regeneration with a natural and synthetic polymer composite [54]. Results of this study have shown similar results even with a more complex soft tissue to be modeled. Scanning electron microscopy (SEM) confirmed that both scaffolds are capable of supporting smooth muscle growth with a confluent layer on each. A slight change in morphology and the extent of confluency was observed but this change may not be caused by a cellular process. There is a possibility that the changes in morphology and confluency on PLLA may be caused by a processing artifacts from drying. PLLA and other polymers shrink when dried, breaking the attachment sights of the cells and causing the breakage seen in the PLLA scaffold. This processing artifact did not seem to affect the cells on the 35 mg/mL PLLA/PLECM scaffold leading us to believe there is a difference with either the scaffolds properties or the cellular layers. There are three possible explanations for this difference. First, there could be little drying artifact and the differences seen are a true morphological difference between the cells. Another explanation would be that multiple layers of cells had built up on the PLLA/PLECM scaffold because of the impact the PLECM has on proliferation, then the top cells seen on ECM would not have been affected by the pulling of the PLLA fibers during drying. Lastly, the PLECM could disrupt the PLLA, lessening the severity of the drying artifact. Morphological differences and signaling changes of smooth muscle

cells with the addition of PLECM is seen in various experiments throughout this research, leading to the conclusion that the visual difference seen in the SEM imaging may not be fully accurate because of processing artifacts but other data would suggest there would be some morphological changes.

It is also important to notice the cellular alignment achieved on both scaffold types. The alignment achievable by the nanofibrous mat without alignment of the scaffold fibers will allow for manipulation of HASMCs into a pattern that will likely promote contraction and dilation of the tube in a circumferential manner [38]. The ability of these electrospun scaffolds to support smooth muscle growth was also supported by Live/Dead staining with a low amount of smooth muscle cell death on 35 mg/mL scaffolds as compared to PLLA with an average 13% more live cells per sample. Increased cell death and a noticeable rounded morphology can be attributed to the lack of signaling proteins in PLLA.

There have been studies of decellularized ECM (DECM) incorporation into nanofiber scaffolds to manipulate stem cell differentiation [37]. From this work and others supporting the positive effect that DECM has on cell phenotype, expression of contractile markers such as αSMA, CNN1, and MYH11 should increase. From our results, similar expressions of these genes except MYH11 were seen between PLLA scaffolds and 35 mg/mL scaffolds. With respect to PLLA and PLECM coatings, PLLA has an increased expression of contractile proteins that does not support our hypothesis. Comparing coatings to electrospun scaffolds provides insight into the role of the topography in phenotypic signaling. Overall there is an increase in contractile protein expression with the exception of MYH11, with electrospun scaffolds. This supports the idea that a fibrous

nanostructure is important in the maintenance of contractile phenotype. While not all of the qPCR data supports our hypothesis, phalloidin staining of F-actin shows a significant difference in arrangement and distribution throughout the cells on PLECM/PLECM scaffolds compared to PLLA only scaffolds. The morphology of the cells and expression of F-actin help to support the idea that PLECM affects cell phenotype.

Throughout the body, active remodeling of ECM occurs in homeostasis, development, and the healing process [55]. The significant increase in expression of genes responsible for the production of important lung ECM proteins such as collagen 1 (COL1 A1) on PLECM/PLLA scaffolds can be attributed to normal remodeling of the scaffold. Collagen 1 production is much less prevalent in PLLA only materials as well as coatings with PLECM. It can be concluded that both ECM structural organization and bioactivity are needed for proper ECM remodeling to occur.

Overall, we were able to develop a fiber diameter distribution most closely resembling the distribution seen in the natural small airway ECM. This is shown clearly in SEM images of the scaffolds and decellularized airway tissue. This research confirmed that PLECM electrospun into the scaffolds results in ECM fragments that are detectable post-electrospinning, seen by SDS-PAGE, Masson's trichrome staining, and collagen and elastin quantification assays. Both elastic modulus and hydrophobicity were confirmed to have decreased drastically to more closely mimic the natural tissue. Lastly we were able to show an increase in bioactivity of the PLECM/PLLA scaffold through cell culture of HBSMCs onto the scaffolds. Cell morphology and viability increased on PLECM/PLLA scaffolds, seen by live dead, SEM, and phalloidin imaging. Gene analysis of contractile

proteins gave insight into the contractility of cells on the scaffolds and concluded that the nanostructure affects the phenotype and ECM production of HBSMCs.

Our future work will include the development more specific bronchiole models to include mechanical stresses with the use of a bioreactor. This research will also be applied to a multicellular model that takes this proven scaffold and modifies fiber diameter and denseness to create optimal epithelial and fibroblast environments for a whole bronchiole tissue model. The current scaffold has shown to be an appealing scaffold for smooth muscle modeling and tissue engineering which can eventually be expanded to investigate cell-cell interactions among multiple cell types as well as the role they play in diseased states.

CHAPTER 5: Conclusion

In this study, we sought to evaluate the potential of a copolymer electrospun nanofiber scaffold consisting of poly-L-lactic acid (PLLA) and decellularized pig lung extracellular matrix (PLECM) as an in vitro airway smooth muscle (ASM) model. We hypothesized that electrospun scaffolds composed of PLECM and PLLA would enhance the bioactivity, mechanical properties, and architecture as compared to scaffolds solely composed of PLLA or PLECM. We were able to verify the presence of key ECM components post electrospinning through histological staining and SDS-PAGE methods. Confirmation of ECM proteins supports the evidence that the bioactivity of this scaffold can be attributed to cell recognition of ECM protein fragments. Additionally, by creating a scaffold that was more similar in mechanical properties and hydrophilicity to human lung tissue, both cell attachment and maintenance of ASM phenotype increase, making it a more beneficial model of the physiological environment. Overall, the electrospun PLLA and PLECM scaffolds promote growth and attachment of HBSMCs, with proves that this combination of natural and synthetic materials are appealing for a tunable *in vitro* ASM model for investigation of natural or disease states.

CHAPTER 6: Supplemental Data and Future Directions

The future directions of this project include the broadening of this scaffold's possible applications. For this scaffold to be used for the modeling of other airway diseases or as regenerative material for lung regrowth after injury, the scaffold must be able to support growth of more cell types than smooth muscle cells. This scaffold's structural characteristics are currently optimized for the growth and differentiation of smooth muscle cells, but if the structural properties were modified, this scaffold could be beneficial for the growth of other cell types. DPLECM includes ECM proteins of the entire small airway and therefore should maintain differentiation of all lung cell linages. As a supplement to the smooth muscle modeling thesis, my research investigated the optimization of this scaffold for mostly Small Airway Epithelial cells (SAECs) but also other airway cell types such as human mesenchymal stem cells (HMSCs), lung fibroblasts, and immortalized lung epithelial cells (A549s).

The first step of SAEC investigation was to look at the response of SAECs on the original scaffold. Figure 19 includes SEM imaging of SAECs cultured on both PLLA and PLECM/PLLA scaffolds for 48 hours showing that both scaffolds support SAEC attachment and growth. 35 mg/mL PLECM scaffold show a slight increase in cell spreading achieving a cobblestone effect compared to the PLLA only scaffold but, overall, there does not seem to be an increase in cell attachment between the two.

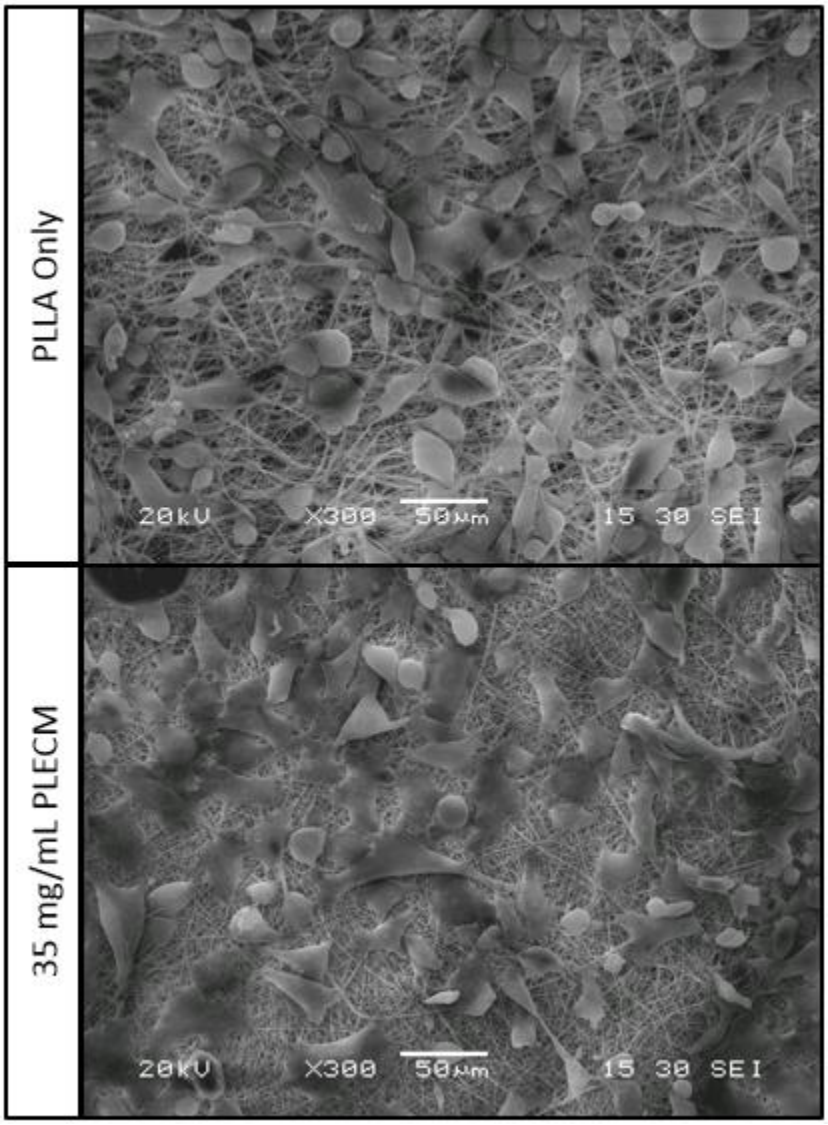

Figure 19: SEM of SAECs on original PLLA/PLECM scaffolds cultured for 48 hours.

SEM of SAECs looked to be encouraging results but was not enough evidence to confirm this scaffold as a effect model for epithelial modeling. To quantify cell proliferation, Picogreen (DNA) proliferation assay was run on SAECs in the same condition and we were able to quantitativly show that there was an increase in cellular proliferation as shown in Figure 20. In this figure, it is easy to determine that PLECM had

a significantly positive affect on proliferation. We also determined that 35 mg/mL showed to be a more benifical concentration of PLECM over 17.5 mg/mL, leading to the disscontinution of 17.5 mg/mL scaffolds in our experiments.

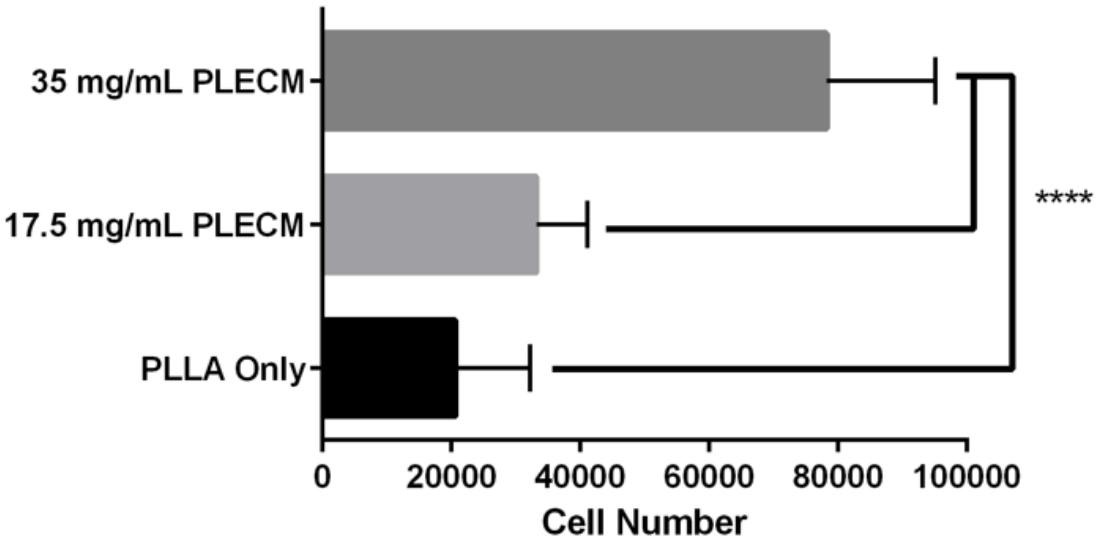

Figure 20: Picogreen (DNA) proliferation assay on SAECs cultured on scaffolds for 48 hours. 6 to 8 samples for each group were seeded with 30,000 cells/cm^3. Values normalized to scaffolds without cells. **** $p<0.0001$

Once the bioactivity was examined this far, a coculture study was done with SAECs and HBSMCs. HBSMCs were cultured one week before seeding SAECs ontop for one more week. The resulting 2 week culture was imaged with phalloidin and DAPI to show the interaction and organization of these two cell types, seen in Figure 21.

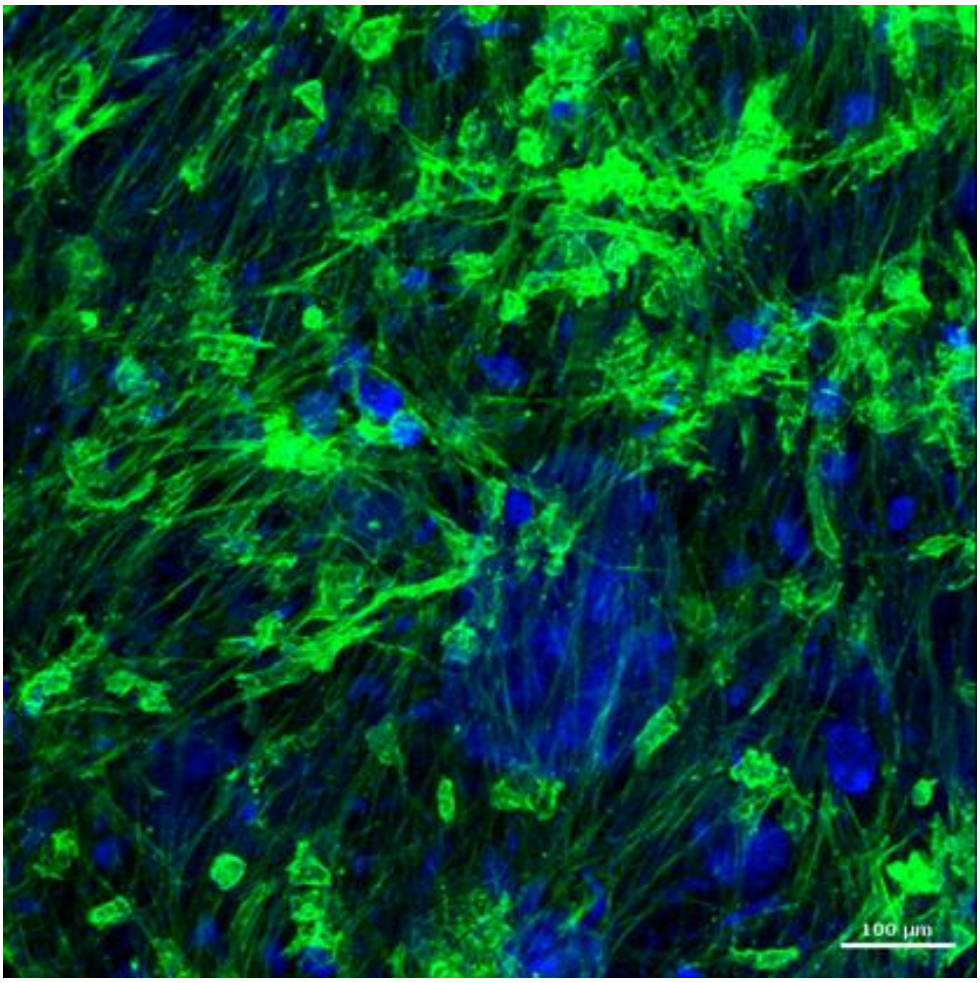

Figure 21: Cocutlure of SAECs and HBSMCs on 35 mg/mL scaffold. HBSMCS were cultured for 1 week before adding SAECs for an additional week and stained with Phalloidin (green) and DAPI (blue).

After coculture studies, more bioactivity and pheotyping studies were done with SAECs on the orginal scaffolds showing results that were no longer supporting our hypothesis that our PLECM/PLLA scaffold would promote SAEC growth. The design of the scaffold then had to be modified to decrease fiber diameter and increase fiber density to more resemble the basement membrane [35]. We tried to more closely mimic a basement

membrane by applying a previously tested [39] The scaffold and hydrogel material has a surface with a denser arrangment of fibers with surrounding environment with high water content, as seen in natrual tissue. Having the original electrospun scaffold on the oppisite side kept the fiber structure and aragement most benificual for smooth muscle culture if coculture studies were desired in the future. The resulting scaffold (Figure 22) was fabricated by adding a pregel solution [39] and allowing to crosslink at 37° C and cultured with SAECs for 48 hours to assess attachment and morphology (Figure 23). The scaffold that was produced showed and increased density to allow for a denser arrangement of fibers. SEM of cultured cells on hydrogel scaffolds showed that it supported SAEC growth but with less cell spreading and attachment than expected.

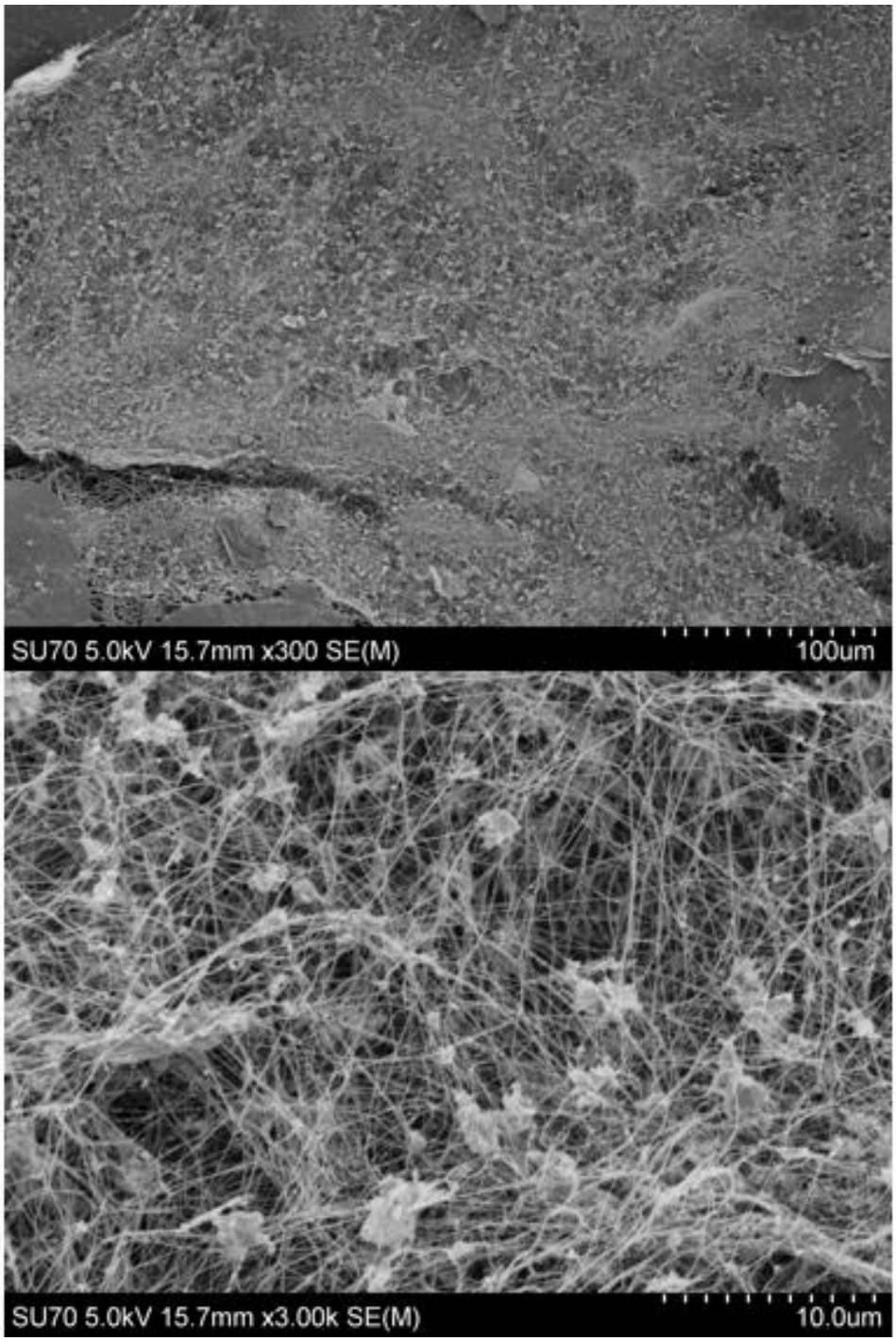

Figure 22: Electrospun PLECM/PLLA scaffold with addtion of ECM hydrogel [39].

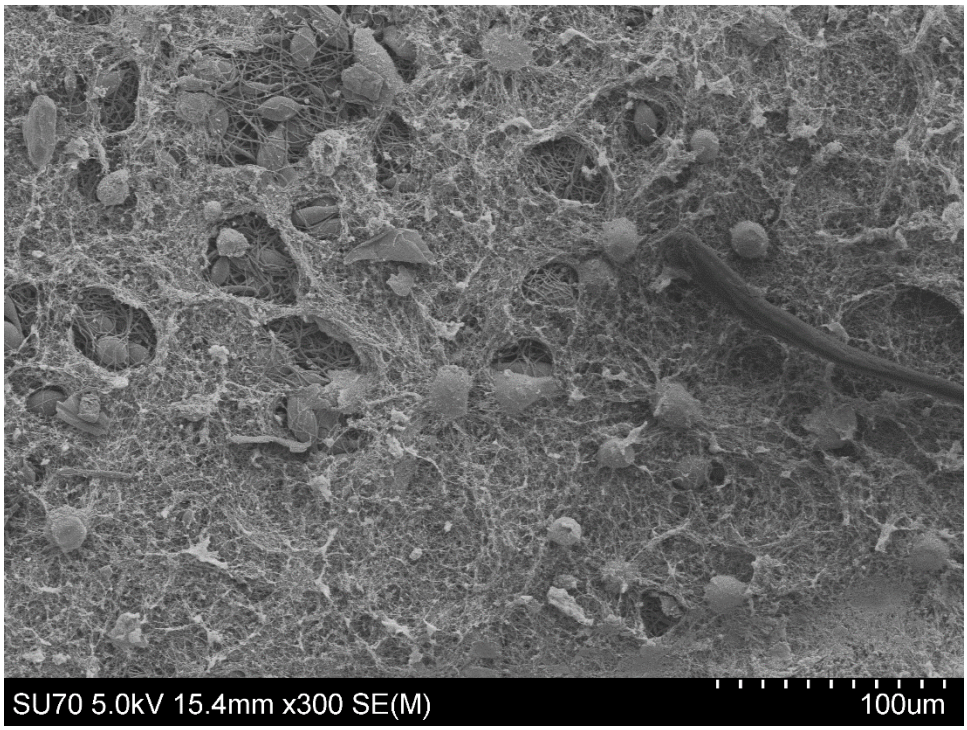

Figure 23: Culture of SAECs onto Electrospun PLECM/PLLA scaffold with hydrogel surface.

In order to test this scaffold as a model for applications that include the modeling of cell types other than smooth muscle cells, we investigated the ability of the scaffold to support airway cell types such as HMSCs, lung fibroblasts, and A549s. HMSCs were cultured onto scaffolds in HMSC high performance media (Rooster Bio, Figure 24) in order to evaluate if the bioactivity of the scaffold alone could differentiate the mesenchymal cells into a definite airway cell type like smooth muscle cells. Cell phenotype was difficult to definitively determine so we relied on qPCR to see if we were seeing an increase in contractile phenotypes as compared to HMSCs not on scaffolds. From the qPCR data (not shown) we were not able to conclude that phenotype was being

driven by the scaffold and more troubleshooting and testing must be done in the future to investigate the effect the scaffold has on HMSCs.

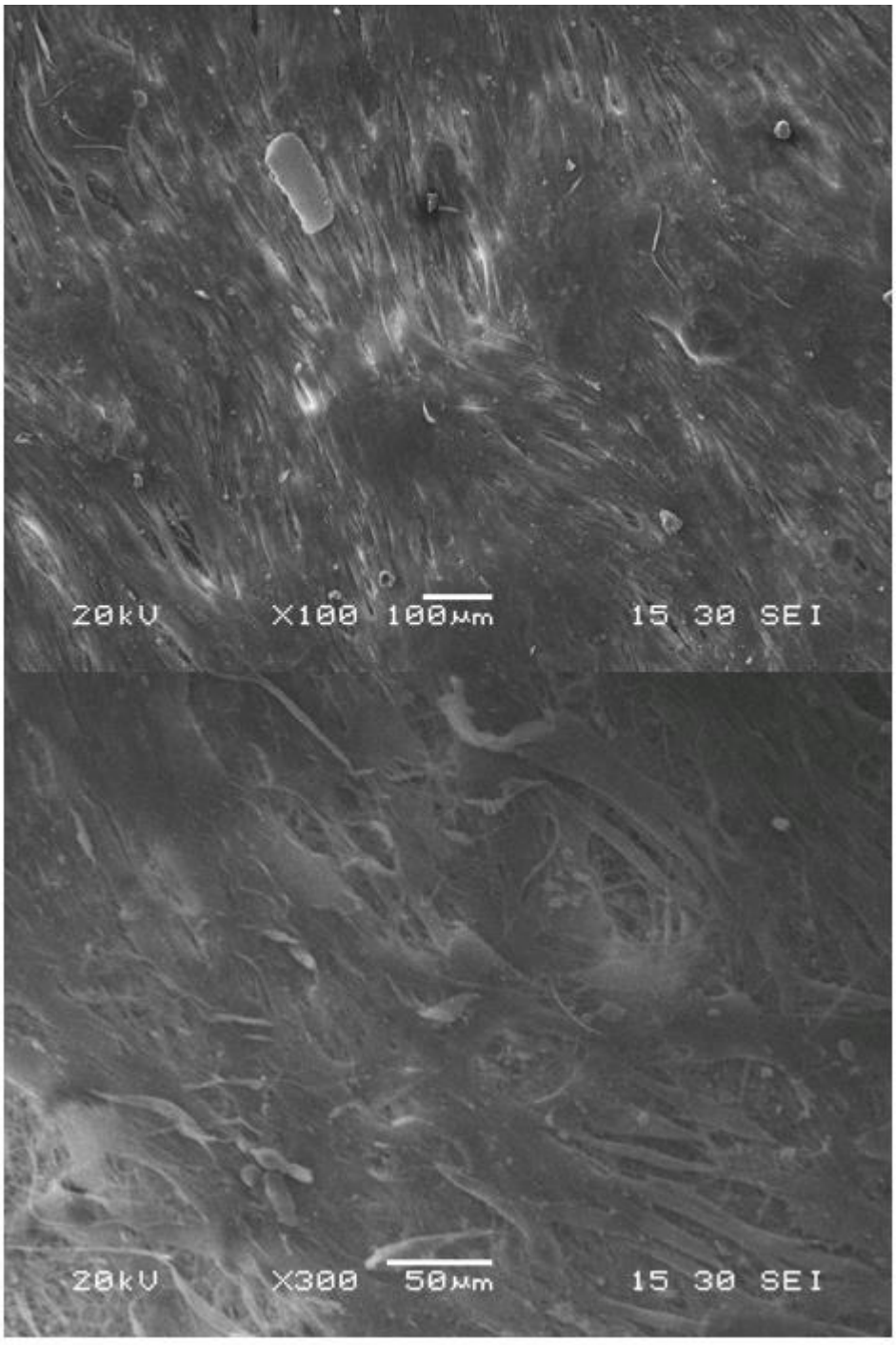

Figure 24: HMSCs cultured onto scaffolds to show stem cell differentiation encouraged by scaffold bioactivity.

To ensure that we looked at the behavior of most cell types within the lung with the scaffold, we also tested the interaction of lung fibroblasts (Figure 25-A) and A549 cells (Figure 25-B). As expected with these two hardy cell types, there was good cell attachment and cell spreading on the scaffold. Especially with the lung fibroblasts because of their similar structural preferences as smooth muscle cells [35], the similar behavioral response was expected.

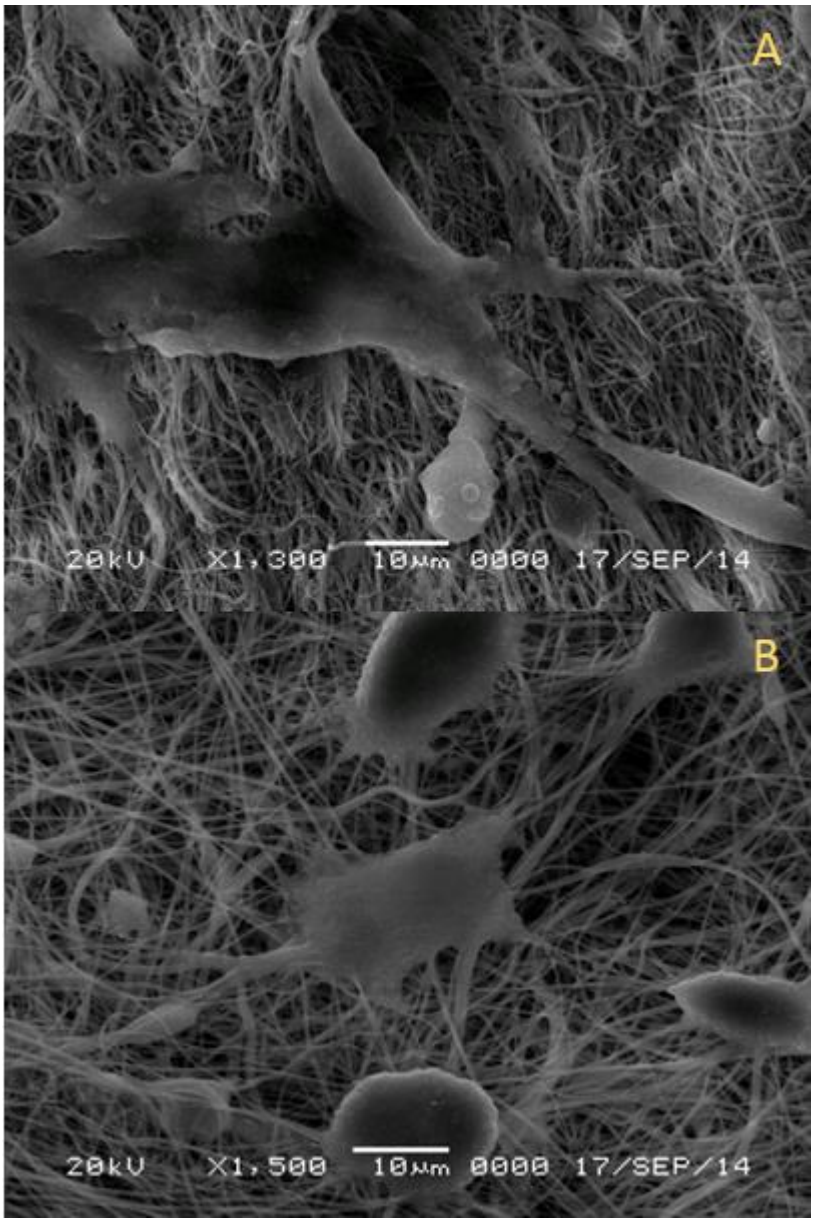

Figure 25: Culture of lung fibroblasts (A) and A549 cells (B) onto 35 mg/mL PLECM scaffolds.

We also looked into bettering our small airway model by creating a more holistic and physiologically environment for culturing the electrospun scaffolds in. The first step was to develop a 3D tube shaped scaffold that more closely resembled the

microarchitecture of the small airways shown in Figure 26-A. A bioreactor prototype was also developed for seeding and culturing of airway cell types was developed and can be seen in Figure 26 B-C. It was comprised of two chambers, on to hold the bronchiole scaffold and the other was a media reservoir. It was equipped with in and out tubing allowing flow between the two holding chambers. This prototype was run with 1.3 million HBSMCs in culture for two weeks. Resulting scaffolds were imaged by SEM but very few cells had attached. We concluded that the flow rate and bioreactor surface area was not optimal for cell culture. Other bioreactor options will be looked at in the future to allow for cell seeding and physiologically relevant culturing that includes airflow through the inside of the tube with pulsatile pressure and media around the outside to function a blood circulation.

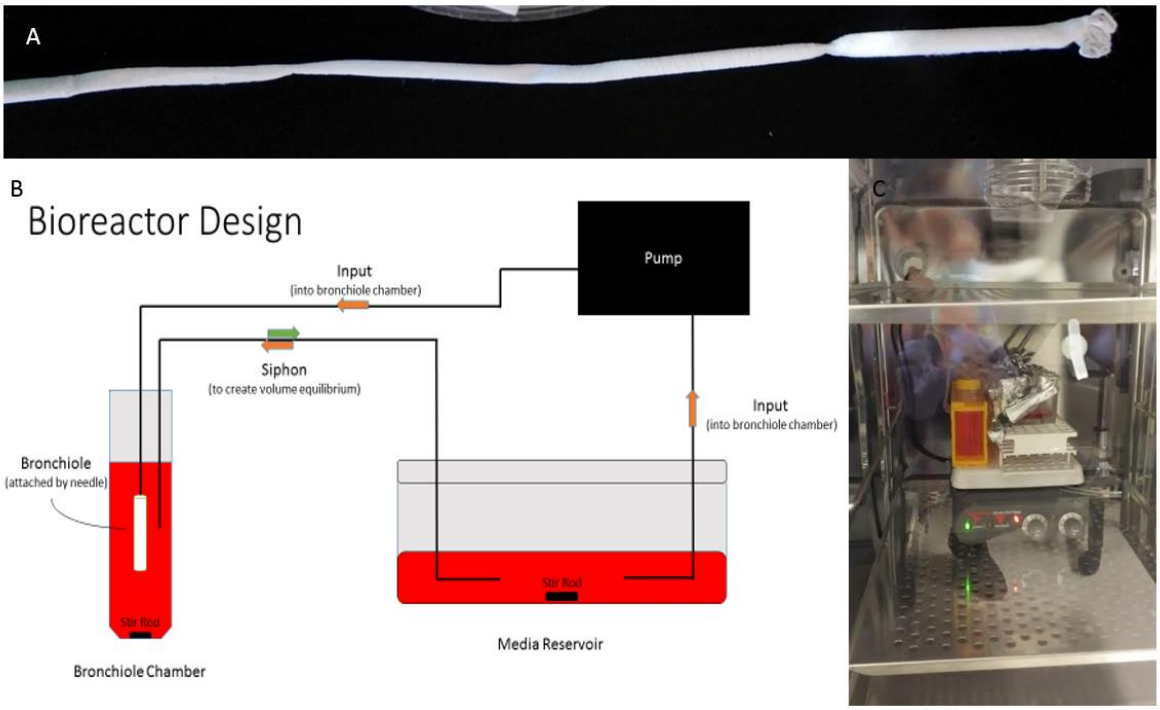

Figure 24

Figure 26: Initial 3D electrospun tube and bioreactor design and setup. 3D electrospun scaffold resembling shape and diameter of bronchiole (A). Planned prototype set up with all all parts labeled (B). The actual set up of the bioreactor in the incubator (C).

References

[1] "American Thoracic Society - Anatomy and Function of the Normal Lung." [Online]. Available: https://www.thoracic.org/copd-guidelines/for-patients/anatomy-and-function-of-the-normal-lung.php. [Accessed: 12-May-2016].

[2] M. Levitzky, *Pulmonary Physiology*, 8th ed. McGraw-Hill, 2013.

[3] R. D. Kamm, "Airway Wall Mechanics," *Annu. Rev. Biomed. Eng.*, vol. 1, no. 1, pp. 47–72, Aug. 1999.

[4] M. Kucki, J.-P. Kaiser, M. J. D. Clift, B. Rothen-Rutishauser, A. Petri-Fink, and P. Wick, "The Role of the Protein Corona in Fiber Structure-Activity Relationships," *Fibers*, vol. 2, no. 3, pp. 187–210, Jun. 2014.

[5] R. Pawankar, S. Holgate, W. Canonica, R. Lockey, and M. Blaiss, "WAO White Book on Allergy." WAO, 2013.

[6] T. Welte and D. A. Groneberg, "Asthma and COPD," *Exp. Toxicol. Pathol.*, vol. 57, Supplement 2, pp. 35–40, Jun. 2006.

[7] D. S. Postma and H. a. M. Kerstjens, "Characteristics of Airway Hyperresponsiveness in Asthma and Chronic Obstructive Pulmonary Disease," *Am. J. Respir. Crit. Care Med.*, vol. 158, no. supplement_2, pp. S187–S192, Nov. 1998.

[8] J. E. Allen, R. J. Bischof, H.-Y. Sucie Chang, J. A. Hirota, S. J. Hirst, M. D. Inman, W. Mitzner, and T. E. Sutherland, "Animal models of airway inflammation and airway smooth muscle remodelling in asthma," *Pulm. Pharmacol. Ther.*, vol. 22, no. 5, pp. 455–465, Oct. 2009.

[9] S. T. Holgate, "Pathogenesis of Asthma," *Clin. Exp. Allergy*, vol. 38, no. 6, pp. 872–897, Jun. 2008.

[10] "Asthma Causes - Mayo Clinic." [Online]. Available: http://www.mayoclinic.org/diseases-conditions/asthma/basics/causes/con-20026992. [Accessed: 12-May-2016].

[11] "Asthma explained - A model for understanding inflammation - NaturalNews.com." [Online]. Available: http://www.naturalnews.com/035291_asthma_inflammation_treatments.html. [Accessed: 12-May-2016].

[12] K. F. Rabe, S. Hurd, A. Anzueto, P. J. Barnes, S. A. Buist, P. Calverley, Y. Fukuchi, C. Jenkins, R. Rodriguez-Roisin, C. van Weel, and J. Zielinski, "Global Strategy for the Diagnosis, Management, and Prevention of Chronic Obstructive Pulmonary Disease," *Am. J. Respir. Crit. Care Med.*, vol. 176, no. 6, pp. 532–555, Sep. 2007.

[13] K. F. Chung, "The Role of Airway Smooth Muscle in the Pathogenesis of Airway Wall Remodeling in Chronic Obstructive Pulmonary Disease," *Proc. Am. Thorac. Soc.*, vol. 2, no. 4, pp. 347–354, Nov. 2005.

[14] D. C. Grootendorst and K. F. Rabe, "Mechanisms of Bronchial Hyperreactivity in Asthma and Chronic Obstructive Pulmonary Disease," *Proc. Am. Thorac. Soc.*, vol. 1, no. 2, pp. 77–87, Apr. 2004.

[15] P. J. Barnes, "Mechanisms in copd*: Differences from asthma," *Chest*, vol. 117, no. 2_suppl, p. 10S–14S, Feb. 2000.

[16] P. J. Barnes, "Immunology of asthma and chronic obstructive pulmonary disease," *Nat. Rev. Immunol.*, vol. 8, no. 3, pp. 183–192, Mar. 2008.

[17] Y. Amrani and R. A. Panettieri, "Airway smooth muscle: contraction and beyond," *Int. J. Biochem. Cell Biol.*, vol. 35, no. 3, pp. 272–276, Mar. 2003.

[18] E. C. Jesudason, "Airway smooth muscle: an architect of the lung?," *Thorax*, vol. 64, no. 6, pp. 541–545, Jun. 2009.

[19] W. Zhang and S. J. Gunst, "Interactions of Airway Smooth Muscle Cells with Their Tissue Matrix," *Proc. Am. Thorac. Soc.*, vol. 5, no. 1, pp. 32–39, Jan. 2008.

[20] A. J. Halayko and J. Solway, "Invited Review: Molecular mechanisms of phenotypic plasticity in smooth muscle cells," *J. Appl. Physiol.*, vol. 90, no. 1, pp. 358–368, Jan. 2001.

[21] S. J. Hirst, C. H. C. Twort, and T. H. Lee, "Differential Effects of Extracellular Matrix Proteins on Human Airway Smooth Muscle Cell Proliferation and Phenotype," *Am. J. Respir. Cell Mol. Biol.*, vol. 23, no. 3, pp. 335–344, Sep. 2000.

[22] L. Bosworth and S. Downes, *Electrospinning for Tissue Regeneration*. Elsevier, 2011.

[23] N. Bhardwaj and S. C. Kundu, "Electrospinning: A fascinating fiber fabrication technique," *Biotechnol. Adv.*, vol. 28, no. 3, pp. 325–347, May 2010.

[24] V. Milleret, B. Simona, P. Neuenschwander, and H. Hall, “Tuning electrospinning parameters for production of 3D-fiber-fleeces with increased porosity for soft tissue engineering applications,” *Eur. Cell. Mater.*, vol. 21, pp. 286–303, 2011.

[25] G. G. Wallace, M. J. Higgins, S. E. Moulton, and C. Wang, “Nanobionics: the impact of nanotechnology on implantable medical bionic devices,” *Nanoscale*, vol. 4, no. 15, pp. 4327–4347, Aug. 2012.

[26] J. D. Stitzel, K. J. Pawlowski, G. E. Wnek, D. G. Simpson, and G. L. Bowlin, “Arterial smooth muscle cell proliferation on a novel biomimicking, biodegradable vascular graft scaffold,” *J. Biomater. Appl.*, vol. 16, no. 1, pp. 22–33, Jul. 2001.

[27] B. Sicari, “CONSTRUCTIVE TISSUE REMODELING BY EXTRACELLULAR MATRIX BIOSCAFFOLDS WITHIN THE AGING SKELETAL MUSCLE MICROENVIRONMENT,” 11-Dec-2013. [Online]. Available: http://d-scholarship.pitt.edu/20257/. [Accessed: 12-May-2016].

[28] P. M. Crapo, C. J. Medberry, J. E. Reing, S. Tottey, Y. van der Merwe, K. E. Jones, and S. F. Badylak, “Biologic scaffolds composed of central nervous system extracellular matrix,” *Biomaterials*, vol. 33, no. 13, pp. 3539–3547, May 2012.

[29] C. O’Leary, B. Cavanagh, R. E. Unger, C. J. Kirkpatrick, S. O’Dea, F. J. O’Brien, and S.-A. Cryan, “The development of a tissue-engineered tracheobronchial epithelial model using a bilayered collagen-hyaluronate scaffold,” *Biomaterials*, vol. 85, pp. 111–127, Apr. 2016.

[30] J. A. Matthews, G. E. Wnek, D. G. Simpson, and G. L. Bowlin, “Electrospinning of collagen nanofibers,” *Biomacromolecules*, vol. 3, no. 2, pp. 232–238, Apr. 2002.

[31] V. M. Merkle, P. L. Tran, M. Hutchinson, K. R. Ammann, K. DeCook, X. Wu, and M. J. Slepian, “Core-shell PVA/gelatin electrospun nanofibers promote human umbilical vein endothelial cell and smooth muscle cell proliferation and migration,” *Acta Biomater.*, vol. 27, pp. 77–87, Nov. 2015.

[32] G. E. Wnek, M. E. Carr, D. G. Simpson, and G. L. Bowlin, “Electrospinning of Nanofiber Fibrinogen Structures,” *Nano Lett.*, vol. 3, no. 2, pp. 213–216, Feb. 2003.

[33] R. Londono and S. F. Badylak, “Biologic Scaffolds for Regenerative Medicine: Mechanisms of In vivo Remodeling,” *Ann. Biomed. Eng.*, vol. 43, no. 3, pp. 577–592, Sep. 2014.

[34] Z.-Q. Feng, H.-J. Lu, M. K. Leach, N.-P. Huang, Y.-C. Wang, C.-J. Liu, and Z.-Z. Gu, “The influence of type-I collagen-coated PLLA aligned nanofibers on growth of

blood outgrowth endothelial cells," *Biomed. Mater. Bristol Engl.*, vol. 5, no. 6, p. 65011, Dec. 2010.

[35] J. C. Bridge, J. W. Aylott, C. E. Brightling, A. M. Ghaemmaghami, A. J. Knox, M. P. Lewis, F. R. A. J. Rose, and G. E. Morris, "Adapting the Electrospinning Process to Provide Three Unique Environments for a Tri-layered In Vitro Model of the Airway Wall," *J. Vis. Exp. JoVE*, no. 101, p. e52986, 2015.

[36] G. E. Morris, J. C. Bridge, L. A. Brace, A. J. Knox, J. W. Aylott, C. E. Brightling, A. M. Ghaemmaghami, and F. R. a. J. Rose, "A novel electrospun biphasic scaffold provides optimal three-dimensional topography for in vitro co-culture of airway epithelial and fibroblast cells," *Biofabrication*, vol. 6, no. 3, p. 35014, Sep. 2014.

[37] M. Gibson, V. Beachley, J. Coburn, P. A. Bandinelli, H.-Q. Mao, J. Elisseeff, M. Gibson, V. Beachley, J. Coburn, P. A. Bandinelli, H.-Q. Mao, and J. Elisseeff, "Tissue Extracellular Matrix Nanoparticle Presentation in Electrospun Nanofibers, Tissue Extracellular Matrix Nanoparticle Presentation in Electrospun Nanofibers," *BioMed Res. Int. BioMed Res. Int.*, vol. 2014, 2014, p. e469120, May 2014.

[38] S. F. Badylak, "Xenogeneic extracellular matrix as a scaffold for tissue reconstruction," *Transpl. Immunol.*, vol. 12, no. 3–4, pp. 367–377, Apr. 2004.

[39] R. A. Pouliot, P. A. Link, N. S. Mikhaiel, M. B. Schneck, M. S. Valentine, F. J. Kamga Gninzeko, J. A. Herbert, M. Sakagami, and R. L. Heise, "Development and characterization of a naturally derived lung extracellular matrix hydrogel," *J. Biomed. Mater. Res. A*, p. n/a-n/a, Apr. 2016.

[40] A. P. Price, K. A. England, A. M. Matson, B. R. Blazar, and A. Panoskaltsis-Mortari, "Development of a Decellularized Lung Bioreactor System for Bioengineering the Lung: The Matrix Reloaded," *Tissue Eng. Part A*, vol. 16, no. 8, pp. 2581–2591, Aug. 2010.

[41] J. L. Long and R. T. Tranquillo, "Elastic fiber production in cardiovascular tissue-equivalents," *Matrix Biol. J. Int. Soc. Matrix Biol.*, vol. 22, no. 4, pp. 339–350, Jun. 2003.

[42] P. Jungebluth, E. Alici, S. Baiguera, P. Blomberg, B. Bozóky, C. Crowley, O. Einarsson, T. Gudbjartsson, S. L. Guyader, G. Henriksson, O. Hermanson, J. E. Juto, B. Leidner, T. Lilja, J. Liska, T. Luedde, V. Lundin, G. Moll, C. Roderburg, S. Strömblad, T. Sutlu, E. Watz, A. Seifalian, and P. Macchiarini, "Tracheobronchial transplantation with a stem-cell-seeded bioartificial nanocomposite: a proof-of-concept study," *The Lancet*, vol. 378, no. 9808, pp. 1997–2004, Dec. 2011.

[43] M. M. Stevens and J. H. George, "Exploring and engineering the cell surface interface," *Science*, vol. 310, no. 5751, pp. 1135–1138, Nov. 2005.

[44] P. J. M. Van Haastert and P. N. Devreotes, "Chemotaxis: signalling the way forward," *Nat. Rev. Mol. Cell Biol.*, vol. 5, no. 8, pp. 626–634, Aug. 2004.

[45] Y. Hong, K. Takanari, N. J. Amoroso, R. Hashizume, E. P. Brennan-Pierce, J. M. Freund, S. F. Badylak, and W. R. Wagner, "An Elastomeric Patch Electrospun from a Blended Solution of Dermal Extracellular Matrix and Biodegradable Polyurethane for Rat Abdominal Wall Repair," *Tissue Eng. Part C Methods*, vol. 18, no. 2, pp. 122–132, Feb. 2012.

[46] J. L. Balestrini and L. E. Niklason, "Extracellular matrix as a driver for lung regeneration," *Ann. Biomed. Eng.*, vol. 43, no. 3, pp. 568–576, Mar. 2015.

[47] L. Bozec, G. van der Heijden, and M. Horton, "Collagen Fibrils: Nanoscale Ropes," *Biophys. J.*, vol. 92, no. 1, pp. 70–75, Jan. 2007.

[48] L. D. Muiznieks, A. S. Weiss, and F. W. Keeley, "Structural disorder and dynamics of elastin," *Biochem. Cell Biol. Biochim. Biol. Cell.*, vol. 88, no. 2, pp. 239–250, Apr. 2010.

[49] L. Huang, R. A. McMillan, R. P. Apkarian, B. Pourdeyhimi, V. P. Conticello, and E. L. Chaikof, "Generation of Synthetic Elastin-Mimetic Small Diameter Fibers and Fiber Networks," *Macromolecules*, vol. 33, no. 8, pp. 2989–2997, Apr. 2000.

[50] T. Courtney, M. S. Sacks, J. Stankus, J. Guan, and W. R. Wagner, "Design and analysis of tissue engineering scaffolds that mimic soft tissue mechanical anisotropy," *Biomaterials*, vol. 27, no. 19, pp. 3631–3638, Jul. 2006.

[51] F. S. A. Cavalcante, S. Ito, K. Brewer, H. Sakai, A. M. Alencar, M. P. Almeida, J. S. Andrade, A. Majumdar, E. P. Ingenito, and B. Suki, "Mechanical interactions between collagen and proteoglycans: implications for the stability of lung tissue," *J. Appl. Physiol. Bethesda Md 1985*, vol. 98, no. 2, pp. 672–679, Feb. 2005.

[52] P. Lu, K. Takai, V. M. Weaver, and Z. Werb, "Extracellular Matrix Degradation and Remodeling in Development and Disease," *Cold Spring Harb. Perspect. Biol.*, vol. 3, no. 12, Dec. 2011.

[53] Y. Arima and H. Iwata, "Effect of wettability and surface functional groups on protein adsorption and cell adhesion using well-defined mixed self-assembled monolayers," *Biomaterials*, vol. 28, no. 20, pp. 3074–3082, Jul. 2007.

[54] J. J. Stankus, D. O. Freytes, S. F. Badylak, and W. R. Wagner, “Hybrid nanofibrous scaffolds from electrospinning of a synthetic biodegradable elastomer and urinary bladder matrix,” *J. Biomater. Sci. Polym. Ed.*, vol. 19, no. 5, pp. 635–652, 2008.

[55] T. R. Cox and J. T. Erler, “Remodeling and homeostasis of the extracellular matrix: implications for fibrotic diseases and cancer,” *Dis. Model. Mech.*, vol. 4, no. 2, pp. 165–178, Mar. 2011.

VITA

Bethany Young was born on December 12, 1991 in Sandusky, Ohio. She graduated from University of Richmond in 2014 with a Bachelor of Science in Biology. During this time she was vice president of Beta Beta Beta, Biological Honor Society and worked at Henrico County Public Works as an engineering technician. Bethany went directly into graduate school at Virginia Commonwealth University in 2014 for Biomedical Engineering. Currently she is a Master of Science degree candidate with research completed in the field of tissue engineering. Her expected graduation is May, 2016.